

Homeodomain protein 1 is an essential regulator of gene expression during sexual differentiation of malaria parasites

Riward Campelo Morillo ¹, Xinran Tong ¹, Wei Xie ², Todd Lenz ³, Gayani Batugedara ³, Nusrat Tabassum ¹, Lindsey M. Orchard ⁴, Wassim Daher ⁵, Dinshaw J. Patel ², William S. Noble ⁶, Manuel Llinás ^{4,7}, Karine G. Le Roch ³, Björn F.C. Kafsack ^{1,*}

¹ Department of Microbiology & Immunology, Weill Cornell Medicine, New York, NY 10065, USA

² Structural Biology Program, Memorial Sloan-Kettering Cancer Center, New York, NY 10065, USA

³ Department of Molecular, Cell and Systems Biology, University of California Riverside, Riverside, CA 92521, USA

⁴ Department of Biochemistry & Molecular Biology and Huck Center for Malaria Research, Pennsylvania State University, University Park, PA, 16802

⁵ Dynamique des Interactions Membranaires Normales et Pathologiques, UMR5235 CNRS, INSERM, Université de Montpellier, Montpellier

⁶ Department of Genome Sciences, University of Washington, Seattle, WA, USA

⁷ Department of Chemistry, Pennsylvania State University, University Park, PA, 16802, USA.

* Corresponding Author: bkafsack@med.cornell.edu

ABSTRACT

Transmission of *Plasmodium falciparum* and other malaria parasites requires differentiation from asexual blood stages into male and female gametocytes, a non-replicative sexual stage necessary for transmission to the mosquito vector. This particular transition relies on chromatin reorganization mechanisms that coordinate the silencing and activation of a large number of stage specific genes. However, the transcriptional and chromatin regulators that mediate the changes during sexual differentiation remain largely unknown. Here, we identify the previously uncharacterized Homeodomain Protein 1 (HDP1) as an essential regulator of this process. HDP1 binds DNA in a sequence-specific manner and is tightly associated with chromatin in early gametocytes and required for the critical expansion of the inner membrane complex. Loss of HDP1 leads to deregulation of heterochromatin-associated gene silencing, decreased telomere clustering and increased chromatin accessibility. We propose that HDP1 plays a crucial role in restructuring the parasite's chromatin landscape during early sexual differentiation.

INTRODUCTION

In order to complete its life cycle, *Plasmodium falciparum*, the most widespread and virulent of the protozoan parasites that cause malaria in humans, must differentiate repeatedly into unique cell types that are able access and exploit specialized niches within their human and mosquito hosts. One of these key developmental transitions occurs during the parasite's blood stage. To maintain a persistent infection within the human host, malaria parasites undergo continuous rounds of asexual replication within erythrocytes. However, these replicating asexual cells are not infectious to their mosquito vector and therefore cannot mediate transmission to the next human host. Transmission requires the formation of non-replicating male and female sexual forms, called gametocytes, that mate in the mosquito midgut after being taken up during a blood meal and develop into the motile ookinete stage that infects the mosquito. While most malaria parasite species form round gametocytes within 2-6 days, sexual differentiation in *P. falciparum* takes substantially longer, 12-14 days, and produces gametocytes with a characteristic falciform morphology that give the parasite its name.

All differentiation requires the repression and activation of genes that underlie the specific phenotypes of the origin and destination cell types, respectively. To ensure commitment to one cell type or another, these transitions are often controlled by a bistable switch that controls the activity of a key regulator at the top of the transcriptional cascade that underlies the differentiation program (Bhattacharya et al., 2010; Norman et al., 2015; Park et al., 2012; Satory et al., 2011). The broader downstream changes in gene expression are then accomplished by both changing the availability of specific transcription factors and changing their access to cell type-specific promoters via chromatin re-organization.

Recent work has found that this paradigm also applies in malaria parasites, where the initiation of sexual differentiation is controlled by bistable expression of a master regulator, the transcription factor AP2-G (Kafsack et al., 2014; Sinha et al., 2014). During asexual replication the *ap2-g* locus is silenced by heterochromatin (Brancucci et al., 2014; Kafsack et al., 2014; Lopez-Rubio et al., 2009) but, due to the presence of AP2-G binding sites within its own promoter region, incomplete repression of *ap2-g* in individual cells can activate a transcriptional feedback loop that drives AP2-G expression to high levels,

thereby committing cells to the gene expression program underlying sexual differentiation (Josling et al., 2020; Kafsack et al., 2014; Poran et al., 2017). Under conditions that impair heterochromatin maintenance, this feedback loop is activated in a larger fraction of cells, thereby increasing the frequency of sexual differentiation (Brancucci et al., 2014; Coleman et al., 2014; Filarsky et al., 2018).

Commitment to the sexual differentiation program also triggers a substantial redistribution of heterochromatin during the early stages gametocyte development (Bunnik et al., 2018; Frschka et al., 2018). These changes involve substantial expansion of subtelomeric heterochromatin domains on several chromosomes to silence asexual blood-stage specific genes. One such example is a cluster of genes on chromosome 2 that are required for trafficking of PfEMP1, a parasite-encoded adhesin on the erythrocyte surface that is critical for immune evasion in asexually-replicating parasites but not expressed in gametocytes (Tibúrcio et al., 2013). Conversely, heterochromatin is lost from several loci that were previously silenced in asexual stages but upregulated during early gametocyte development (Bunnik et al., 2018; Frschka et al., 2018).

While AP2-G is critical for the initiation of sexual differentiation, it is expressed only during a small window beginning with sexually committed schizonts and is no longer required after the first 48 hours of gametocyte development (Bancells et al., 2019; Josling et al., 2020). This suggests that the changes in gene expression underlying gametocyte development are carried out by a second wave of transcriptional regulators, which is consistent with the observation that AP2-G upregulates a number of putative transcription factors and chromatin remodeling enzymes (Josling et al., 2020; Poran et al., 2017).

Unsurprisingly, gametocyte maturation over nearly two weeks and five distinct morphological stages is accompanied by a wide array of gene expression changes (Kent et al., 2018; Painter et al., 2017; van Biljon et al., 2019; Young et al., 2005). However, relatively little is known about the transcriptional regulators downstream of AP2-G that mediate these changes. Compared to other single-celled eukaryotes, the genomes of malaria parasites contain a small fraction of DNA binding proteins. Like AP2-G, most belong to the ApiAP2 family (Balaji et al., 2005), but only a small number have been shown to function specifically during gametocyte development (Modrzynska et al., 2017).

In the rodent malaria parasite *P. berghei* the DNA-binding protein PbAP2-G2 functions as a transcriptional repressor of asexual-specific gene expression (Sinha et al., 2014; Yuda et al., 2015), while PbAP2-FG (PyAP2-G3 in *P. yoelii*) was shown to mediate upregulation of female-specific transcripts (Yuda et al., 2019; Zhang et al., 2017). Whether these functions are conserved in *P. falciparum* remains to be determined.

In this study, we identify HDP1, a previously uncharacterized DNA-binding protein that is upregulated during sexual differentiation. Parasites lacking HDP1 and are unable to upregulate genes required for the expansion of the inner membrane complex and fail to progress beyond the earliest stages of gametocyte development. Additionally, loss of HDP1 expression results in an increase in chromatin accessibility, reduced telomere clustering, and leaky transcription of heterochromatin-associated genes in early gametocytes. Our findings indicate that HDP1 is an essential regulator of gene expression and chromatin during early gametocytogenesis.

RESULTS

***hdp1* is essential for gametocyte development.**

Searching for possible regulators of gene expression during *P. falciparum* sexual differentiation, we identified Homeodomain-like protein 1 (*hdp1*, PF3D7_1466200) encoding a 3078 amino acid protein with a C-terminal homeodomain-like domain, a helix-turn-helix structural motif commonly involved in DNA binding (Figure 1A) (Bürglin and Affolter, 2016). Syntenic orthologs of *hdp1* could readily be identified in other malaria parasites with homology to the homeodomain-like domain extending to the coccidia but apparently absent from other apicomplexan clades (Figure 1B). Analysis of *hdp1* expression in *P. falciparum* blood stages by qRT-PCR detected only minimal expression in asexual blood stages with substantial upregulation during the early stages of gametocytogenesis (Figure 1C). AP2-G, the transcriptional master switch that initiate the sexual differentiation gene expression program (Kafsack et al., 2014), binds at two sites located upstream of *hdp1* coding sequence early during the gametocytogenesis (Josling et al., 2020), consistent with our hypothesis that AP2-G activates additional regulators of gene expression during early gametocytogenesis.

In an effort to determine HDP1's subcellular localization, we inserted an in-frame N-terminal HaloTag at the endogenous locus (Figure S1A) in order to avoid possible interference with the putative DNA-binding activity of the C-terminal homeodomain-like domain. As expected, no Halo-tagged protein could be detected in asexual stages (data not shown). However, when we attempted to determine Halo-HDP1 levels, we found that *halo-hdp1* cultures were unable to produce the characteristic crescent shapes of maturing *P. falciparum* gametocytes (Figure 2A-B). Tagging the HDP1 C-terminus with either GFP or a triple Ty1 epitope tag (*hdp1-gfp* and *hdp1-Ty1*, Figure S1B-C), yielded parasite lines that produce gametocytes indistinguishable in numbers and morphology from the wildtype parent (Figure 2A-B), despite the proximity to the putative DNA-binding domain.

To test whether insertion of the N-terminal tagging resulted in a loss of HDP1 function, we generated a HDP1 knockout line for comparison. We used genome editing to replace 1.4 kb at the 5' end of the *hdp1* locus with a selectable marker cassette (Figure S1D). The resulting $\Delta hdp1$ parasites exhibited no discernible change in phenotype in asexual blood-stages, but like the *halo-hdp1* parasites, were unable to generate falciform gametocytes (Figure 2D-E). More detailed analyses using synchronous induction of gametocytogenesis found that both *halo-hdp1* and $\Delta hdp1$ have sexual commitment rates comparable to the NF54 parent (Figure S2A) but are unable to complete gametocyte development. We found that on day 2 of development $\Delta hdp1$ Stage I gametocytes had normal levels of viability (Figure S2B) as indicated by robust mitochondrial membrane potential but had lost the ability to maintain this potential by day 5 of development when gametocytes from other lines had matured to stage III (Figure 2C, F).

As the substantial length of the *hdp1* coding sequence made genetic complementation infeasible, we generated an inducible *hdp1* knockdown parasite line by inserting a triple Ty1 epitope tag followed by with the autocatalytic glmS ribozyme at the 3' end of the endogenous *hdp1* coding sequence through genome editing (Figure S1E) (Prommana et al., 2013). In the absence of glucosamine, the resulting *hdp1-glmS* gametocytes expressed HDP1 protein at levels comparable to the *hdp1-Ty1* parasites without the ribozyme and produced normal gametocytes in term of number and morphology (Figure S3). Supplementation of the culture medium with 5mM glucosamine during the first 5 days

of gametocyte development had no discernible effect on *hdp1-Ty1* parasites but diminished HDP1 expression by 70% and reduced falciform gametocytes by 80% in *hdp1-glmS* parasites, recapitulating the phenotype of the *halo-hdp1* and $\Delta hdp1$ lines (Figure 2G-H). Since *hdp1* transcript levels remain relatively constant during gametocyte development (Figure 1C), we wanted to test whether continuous expression of HDP1 was required for gametocyte maturation. Knockdown of *hdp1* levels with glucosamine reduced gametocyte maturation when added prior to day 5 but not thereafter, indicating that sufficient HDP1 protein had been produced by that time to support gametocyte maturation (Figure S3).

HDP1 localizes to the nucleus of early gametocytes.

An earlier study had reported a variety of subcellular localizations for HDP1, including export to the erythrocyte membrane of early gametocytes, based on antibodies raised against the low-complexity repeat region (Nixon et al., 2018). This was surprising given the absence of a predicted signal peptide or transmembrane domains and localization of the *Toxoplasma gondii* ortholog to the nucleus of tachyzoites (Figure S4). To resolve this apparent disagreement, we carried out live-cell and immunofluorescence microscopy in gametocytes of *hdp1-gfp* and *hdp1-Ty1*, respectively. In each case, HDP1 clearly localized to the gametocyte nucleus (Figure 3A-B). Analysis of HDP1 protein levels by western blotting of *hdp1-Ty1* lysates with antibodies against the Ty1 epitope tag detected no expression in asexual blood stages but showed increasing HDP1 levels from day 2 of gametocytogenesis (Stage I-II) onward, reaching maximal levels by day 5 (Stage III) before dropping again by day 8 (Stage IV) (Figure 3C). Analysis of subcellular fractions from day 5 *hdp1-Ty1* gametocytes showed HDP1 almost exclusively in the parasite nucleus, where about 70% is resistant to solubilization with up to 600mM NaCl, indicating a tight association with chromatin (Figure 3D) and validating HDP1 as a nuclear protein.

The HDP1 homeodomain-like domain dimerizes to efficiently bind DNA *in vitro*.

To evaluate HDP1's ability to bind DNA, we expressed a GST-fusion of the HDP1 homeodomain in *E. coli*. Following protein isolation, we found that much of the fusion protein remained bound to bacterial DNA but could be released by the addition of the poly-cation polyethylenimine during isolation (*data not shown*). Analysis of the domain's sequence

specificity by protein-binding microarray showed a preference for the palindromic hexamer GTGCAC (Figure 4A, Figure S5). Since homeo-domains generally recognize DNA as dimers (Bürglin and Affolter, 2016; Pradhan et al., 2012), we carried out isothermal titration calorimetry to measure the interaction of HDP1 with double-stranded DNA containing a tandem motif with a 5 bp spacer that places the motifs one helical turn apart. The results indicated optimal binding at 2:1 protein to DNA molar ratio with a dissociation constant of 2.8 μ M supporting DNA recognition as a dimer (Figure 4B). Next, we performed DNA gel-shift assays with double-stranded probes containing either no match, a single binding-motif, or a tandem motif. When compared to the tandem-motif probe, the gel-shift of the single motif probe was substantially weaker but identical in size (Figure 4C), again consistent with DNA recognition as a dimer. Intriguingly, a scan of the 3D7 reference genome for instances of GTGCAC tandem motifs with a 5-6 bp spacer found them exclusively located at each chromosome end with the first tandem located within either 7 or 28bp of the ultimate *rep20* sub-telomeric repeat, with the exception of those ends where this region was deleted as the result of telomere healing events (Calhoun et al., 2017) (Figure 4D, Data Set 1). Earlier work had predicted these conserved sequences to be recognized by the ApiAP2-domain protein SIP2 in asexual blood stages based on its ability to bind them *in vitro* (Flueck et al., 2010), however, their unique spacing and palindromic nature clearly distinguishes these tandem motifs from the arrays of SIP2 binding sites just downstream. While the function of these motifs in asexual and sexual blood stages remains unclear, their exclusive localization at chromosome ends is highly conserved across *P. falciparum* isolates (*data not shown*).

Loss of HDP1 leads to dysregulation of gene expression during early gametocyte development.

Based on HDP1's ability to bind DNA, we wanted to test whether it plays a role in the regulation of gene expression during early gametocytogenesis. To minimize the chance of looking at the consequences of aberrant gametocyte development we decided to sequence total RNA from $\Delta hdp1$ and parental NF54 Stage I gametocytes on Day 2 of development when HDP1 is first expressed but prior to any change in viability or morphology in HDP1 deficient parasites (Figure 2D, Figure S2B).

Global comparison of transcript abundances by RNA-seq showed that the majority of genes were expressed at similar levels including the markers of very early gametocytes *pfs16* and *gexp5* (Figure 5A), supporting our earlier observation that HDP1-deficient parasites initiate gametocyte development at similar rates. However, we observed reduced transcript levels for 188 genes and increased levels for 150 genes in $\Delta hdp1$ Stage I gametocytes compared to those of the NF54 parent line. Gene set enrichment analysis (GSEA) found that transcripts encoding components of the inner membrane complex were significantly down-regulated (Figure 5B) while transcripts from heterochromatin-associated multi-copy gene families were significantly over-represented among up-regulated genes (Figure 5C), including members of the *var*, *rifin*, *stevor*, and *PHISTa/b/c* gene families (Figure 5D, Fig S6A-B). While fold-changes for these genes could be substantial, the absolute increase in transcripts for these genes was often relatively small but significantly above levels in WT cells (Data Set 2), possibly indicating impaired heterochromatin-mediated silencing allowing for leaky background transcription rather than full transcriptional activation. Comparison of transcript levels of *var* and *rifin* family genes found similar levels of upregulation regardless of whether these were located in subtelomeric or non-subtelomeric regions of heterochromatin (Figure S6C). Analysis of *var* gene expression in asexual $\Delta hdp1$ ring-stages found expression of a single major *var* gene as expected for a recently cloned parasite line and indicating that mutually exclusive *var* gene expression remained unaffected (Figure S6D).

Loss of HDP1 increases chromatin accessibility and decreases telomeric clustering in early gametocytes.

Despite numerous attempts with the GFP- and Ty1-tagged lines, we were unable to determine genome-wide binding of HDP1 by chromatin immunoprecipitation sequencing. Instead, we used high-throughput chromatin-conformation capture (Hi-C) to look for differences in chromatin organization of day 2 gametocytes between the NF54 and $\Delta hdp1$ lines. While correlation analysis of Hi-C replicates indicated a clear difference between these lines (Figure 6A), overall intra-chromosomal interactions appeared largely unchanged (Figure S7). However, further statistical analysis revealed a genome-wide reduction in long distance interactions in $\Delta hdp1$ (Figure 6B). Genome-wide mapping of

interaction changes revealed a substantial reduction in interaction frequency between virtually all chromosome ends (Figure 6C), consistent with reduced but not abrogated telomere clustering. Based on the small but significant upregulation of heterochromatin associated genes and a reduction in telomeric clustering, we hypothesized that chromatin compaction might be impaired in HDP1-deficient parasites resulting in increased chromatin accessibility. Indeed, brief treatment with micrococcal nuclease (MNase) revealed accelerated digestion of chromatin from $\Delta hdp1$ gametocytes (Figure 6D), consistent with an increase in chromatin accessibility.

HDP1 is required for extension of the inner membrane complex in early gametocytes.

Among the genes with reduced transcript levels in HDP1 knockout parasites, those associated with the inner membrane complex were substantially enriched (Figure 5A-B, Figure 7A). This was notable since $\Delta hdp1$ gametocytes fail to elongate from spherical stage I gametocytes into the oblong Stage II, a process that depends on the extension of the inner membrane complex. Six separate inner membrane complex genes were confirmed by qRT-PCR to have greater than 2-fold lower transcript levels in HDP1 knockout gametocytes (Figure 7B). These included PhIL1 and the PhIL1-interacting protein 1 (PIP1), both of which are highly upregulated in early *P. falciparum* gametocytes and essential for inner membrane complex assembly and gametocyte maturation (Parkyn Schneider et al., 2017). Strikingly, the spherical morphology of $hdp1$ -deficient gametocytes perfectly resembles the phenotype of gametocytes when PhIL1 is knocked down. Comparison of PhIL1 protein levels showed a 75% percent reduction in $\Delta hdp1$ gametocytes compared to wild-type parent (Figure 7C). The concomitant reduction in PhIL1 expression (Figure 7D) and inner membrane complex extension (Figure 7E) when HDP1 is knocked down with glucosamine in $hdp1-glmS$ gametocytes confirmed the dependence of PhIL1 expression on HDP1.

DISCUSSION

Our understanding of the regulatory mechanisms that control sexual differentiation in *P. falciparum* has improved substantially in recent years. Much of this work has focused on the regulation of AP2-G, the master regulator of this developmental decision. However, it is becoming clear that the function of AP2-G is constrained to the initiation of the transcriptional program that underlies the nearly two week-long process of forming gametocytes (Bancells et al., 2019). This suggests that a second wave of hitherto unknown transcriptional regulators is required to drive gametocyte-specific gene expression during early gametocyte development.

In this study, we demonstrate that HDP1 functions as an essential regulator during sexual differentiation. A nuclear DNA-binding protein, HDP1 is specifically up-regulated during early gametocyte development and essential for their maturation. In particular, HDP1 regulates the expression of genes required for the expansion of the inner membrane complex that gives *P. falciparum* gametocytes their characteristic crescent shape. While HDP1 expression in *P. falciparum* is gametocyte specific, its *P. berghei* ortholog (PBANKA_1329600) may also function during asexual blood-stage replication as its disruption leads to significant reduction in growth. This suggests that the gametocyte-specific function of HDP1 may have evolved more recently in the Laveranian clade of malaria parasites which produce crescent gametocytes. While absent from the asexual blood-stages and essential during early gametocyte development, whether HDP1 is required in other parasite stages remains to be determined. Since the knockdown system used in this study regulates expression at the transcript level, we can infer that additional translation of HDP1 is not required during the later stages of gametocyte maturation but HDP1 protein expressed during the earlier stages may well be required throughout gametocyte development. Previous transcriptomic studies indicate that HDP1 is also expressed in ookinetes, suggesting a role even following mating. Intriguingly, homeodomain-like proteins have been implicated in mating processes of other haploid protozoa, such as *Dictyostelium* (Hedgethorpe et al., 2017).

We also found that HDP1 is required for efficient heterochromatin-mediated gene silencing during sexual differentiation. In gametocytes lacking HDP1, we observed low

but significant up-regulation across a wide array of heterochromatin-associated gene families. Chromosome conformation capture analysis showed broad alterations to chromatin organization in HDP1-deficient parasites with an overall reduction in long-distance interactions that was most pronounced at the end of chromosomes, consistent with reduced, but not ablated, clustering of the sub-telomeric heterochromatin regions in the nuclear periphery. While its cognate DNA motifs are exclusively found at the boundary of the subtelomeric repeats, localization of HDP1 appeared evenly distributed throughout the gametocyte nucleus rather than in foci at the nuclear periphery, suggesting that the HDP1 does not localize to these sites exclusively. One explanation is that HDP1 promotes chromatin packaging, leading to an overall increase in chromatin accessibility observed in HDP1 deficient cells. This would also explain the leaky expression of heterochromatin-associated genes as efficient silencing depends on limiting promoter accessibility while the promoters of euchromatin-associated genes are already generally accessible and a reduction in packaging would therefore be predicted to have little impact on transcript levels.

Additional studies will focus on identifying interaction partners of HDP1 and elucidating its the structure-function relationship. Only 2% of its protein sequence is comprised of the homeodomain-like DNA-binding domain while the remainder contains no other identifiable domains and conservation is generally weak outside this region. The fact that insertion of a large tag at the N-terminus results in loss of function indicates that critical interactions occur in this region but which other regions are essential for HDP1's function remains unclear. Similarly, identifying interactions with other nuclear proteins and genomic locations will offer important insights into its function. Of particular interest will be whether HDP1 regulates gene expression by altering chromatin structure or is more directly involved in the recruitment of RNA polymerase.

MATERIALS & METHODS

Parasite culture

Unless otherwise noted, parasite strains were grown in 0.5% AlbuMAX II supplemented malaria complete medium using established cell culture techniques (Moll et al., 2008) at 3% hematocrit and below 3% parasitemia. Strains expressing selectable markers were maintained under constant drug-selection. Toxoplasma tachyzoites were cultured as described in (Morlon-Guyot et al., 2018).

Gametocyte induction

Gametocytes were induced synchronously as previously described in (Poran et al., 2017). Gametocyte maturation was monitored by Giemsa-stained thin blood smears and gametocytemia was counted on the fifth day of development. The gametocyte commitment rate was calculated by dividing the day 5 gametocytemia by the day 1 parasitemia, counted before addition of N-acetyl-D-glucosamine. Gametocytes were purified from culture at the required development stage using magnetic columns (LS columns, Miltenyi Biotec). For knockdown experiments in the HDP1-glmS line, at the gametoring stage and either 5 mM glucosamine or solvent control was added.

Generation of transgenic strains

Transfection of ring-stage parasites were performed as previously described (Rug and Maier, 2012) and selected on 4nM WR99210 and 1.5 μ M DSM1 for two weeks. To obtain $\Delta hdp1$ parasites, selection with WR99210 was kept all the time. Genome editing was performed by CRISPR/Cas9 technology using the system described by (Ghorbal et al., 2014). The pL6-DX2 plasmid, containing the sgRNA-expression cassette and the positive selectable marker cassette (*cam* promoter-*hdhfr-hrp2*/ts 3'utr) was used as backbone. Homology boxes were PCR amplified from NF54 genomic DNA, using specific primers flanked by appropriate overlapping region from pL6-DX2 plasmid (list of primers, see Supplementary Table) that allowed the cloning by Gibson assembly. All PCR reactions were set using Advantage Genomic LA polymerase (Takara, Cat. N° 639152). *Plasmodium* codon optimized sequences for HALO-tag and triple Ty1 epitope tag were synthesized as gene-Blocks (Genewiz). PCR products were purified from agarose gel using the Zymoclean Gel DNA Recovery Kit (Zymo Research, Cat. N° D4008). Homology boxes were cloned through *AflIII* and *SpeI* cutting sites, while annealed oligonucleotides paired encoding sgRNA with targeting sequence (Table) were inserted through the *XhoI* site, placed upstream of the sgRNA scaffold sequence. Sanger sequencing confirmed the absence of undesired mutations in the homology boxes and the sgRNA. Genomic DNA from transfectant parasites was isolated

with QIAamp DNA blood Kit (Qiagen, Cat. N° 51106) and diagnostic PCR's were set using Taq phusion DNA polymerase (Invitrogen). The TGME49_233160-HA parasite line was generated as part of an earlier study by tagging of the endogenous locus in the *T. gondii* RH-ku80ko strain as described in (Morlon-Guyot et al., 2018).

Flow cytometric analysis of gametocyte viability

Gametocytes were stained with 16 μ M Hoechst33342 and 50 nM DiIC1 for 30min at 37°C. Using a Cytex DXP12 flow cytometer, gametocytemia was determined by gating for DNA-positive, hemozoin-high cells and gametocyte viability was inferred based on mitochondrial membrane potential dependent accumulation of DiIC1(5) for 1000 gametocytes (Tanaka and Williamson, 2011).

Nuclear extract preparation and high salt fractionation

Nuclear enriched fraction was prepared following the protocol previously described in (Flueck et al., 2009), with some modifications. Briefly, parasites released from RBC's by saponin treatment (0.01%) were lysed with ice-chilled CLB (20mM HEPES pH 7.9; 10mM KCl; 1mM EDTA pH 8.0; 1mM EGTA pH 8.0; 0.65% NP-40; 1mM DTT, 1x Roche Complete protease inhibitors cocktail). Nuclei were pelleted at 3,000 x *g* for 20min at 4°C and cytoplasmic fraction was removed. Nuclei were resuspended in digestion buffer (20mM Tris- HCl, pH 7.5, 15mM NaCl, 60mM KCl, 1mM CaCl₂, 5mM MgCl₂, 300mM sucrose, 0.4% NP-40, 1mM DTT, 1x Roche Complete protease inhibitors cocktail EDTA-free) and treated with 5U of micrococcal nuclease (ThermoFisher, Cat. N° 88216) for 30 min in a water bath at 37°C. Soluble and insoluble nuclear fractions were recovered by centrifugation at 3,000 x *g* for 10 min at 4° C. Insoluble nuclear fraction were treated with salt fractionation buffer (10mM Tris HCl pH 7.4; 2mM MgCl₂; 2mM EGTA pH 8.0; 0.1% Triton X-100; 0.1mM PMSF; 1x Roche Complete protease inhibitors cocktail) supplemented with increasing NaCl concentrations (80-600mM) while rotating at 4°C for 30 min. All supernatants were recovered by centrifugation at 700 x *g* for 4 min at 4°C and last remaining pellet was resuspended in 1x PBS supplemented with protease inhibitors cocktail. 5% of each fraction was prepared for Western blotting in order to check quality of fractionation.

Immunoblotting

For SDS-PAGE, total protein lysates were prepared using saponin-lysed parasites resuspended with 1x Laemmli loading buffer diluted in 1x PBS supplemented with 1x Roche Complete protease inhibitors cocktail. Protein samples were separated in 4-15% polyacrylamide gels and transferred to 0.2 μ m Immobilon-P^{SQ} transfer membrane (Millipore, Cat. No ISEQ00010) using a Bio-Rad

transfer system. Membranes were blocked in 5% skim milk/1x TBS-Tween20 for 1 hour at RT. Primary and secondary antibodies were prepared in 3% skim milk/1x TBS-Tween20 and incubated for 1 hour at RT. Membranes were washed four times with 1x TBS-Tween20 for 10 min, after primary and secondary antibody incubations. The following primary antibodies were used in this study: Anti-Ty1 BB2 mouse (1:2,500; Invitrogen Cat. N° MA5-23513), anti-Phil1 rabbit (1:5,000 (Saini et al., 2017)), anti-PfHsp70 rabbit (1:5,000; StreetsMarq Biosciences Cat. N° SPC-186D), anti-Histone 4 rabbit (1:2,000; Diagenode Cat. N° C15410156-50). HRP-conjugated anti-mouse and anti-rabbit antibodies were used (1:5,000, Millipore). Immunoblots were incubated with the chemiluminescent substrate SuperSignal West Pico PLUS (ThermoFisher, Cat. N° 34578) following manufacturer directions. Images were obtained using Azure c300 digital imaging system (Azure Biosystems).

Live-cell and Immunofluorescence microscopy

For live-cell microscopy of *hdp1-gfp* and NF54 gametocytes, infected red blood cells were stained with 16 µM Hoechst33342 in incomplete media for 15 min at 37° C and imaged at 1000× magnification using a Leica DMI6000 microscope with differential interference contrast bright field optics, DAPI, and GFP filter cubes with identical exposure times.

For immunofluorescence microscopy of *hdp1-Ty1* and *hdp1-glmS* gametocytes, cells were seeded onto slides with Concanavilin A (5mg/ml; Sigma) as described in (Mehnert et al., 2019), then fixed with a solution of 4% paraformaldehyde/0.0075% glutaraldehyde for 20 min at 37° C. Parasites were permeabilized with 0.1% Triton X-100 for 15 min at RT followed by blocking with 3% BSA. Primary antibodies (anti-Ty1 BB2 mouse 1:1,000; anti-Phil1 rabbit 1:400) were allowed to bind for 1 hour in 3% BSA/PBS followed by three washes with blocking buffer for 5 min. Secondary antibodies diluted 1:500 (anti-mouse-Alexa546 and anti-rabbit-Alexa488, Invitrogen) plus 16 µM Hoechst33342 were added in fresh blocking buffer and incubated for 1 hour. Z-stacks of stained specimens were collected at 1000× magnification using a Leica DMI6000 microscope with differential interference contrast bright field optics, DAPI, and RFP filter cubes with identical exposure times. Fluorescent channel z-stacks were deconvolved using the ImageJ DeconvolutionLab2 plugin (NLLS algorithm) followed by maximum intensity z-projection and background adjustment. Immunofluorescence microscopy of *Toxoplasma* tachyzoites was carried out as previously described (Morlon-Guyot et al., 2018).

Protein Expression and Purification

Expression of recombinant HDP1-DBD motif was done using the Glutathione S-transferase (GST) gene fusion system (GE, Healthcare). The pGEX-4T-1 (Addgene Cat. N° 27458001) plasmid was used as backbone for cloning the codon optimized sequence comprising the last 87aa of HDP1. Plasmid pGEX-GST-HDP1-DBD was transformed into BL21 (DE3) competent *E. coli* strain (NEB, Cat. N° C2527) and protein expression was done following the manufacturer directions with some modifications. Briefly, an overnight culture was inoculated with one bacterial colony in 2x YT media supplemented with the corresponding antibiotic. Next day, culture was diluted 1:100 with fresh media and kept at 30° C with vigorous agitation. Bacterial growth was monitored until culture reach exponential phase. At this point, IPTG (1mM final concentration) was added and the culture was kept for another 2 hours at 30° C with vigorous agitation. Cells were harvested and resuspended in lysis buffer (50mM Tris HCl pH 7.5; 100mM NaCl; 1mM DTT; 5% Glycerol; 1mM PMSF; 1mM EDTA; 1x protease inhibitors cocktail) supplemented with Lysozyme (1mg/ml, Sigma). In order to remove bacterial DNA from our putative DNA binding protein, lysate was treated with polyethyleneimine (PEI) (0.1% v/v) (RR, 1991). Lysate was sonicated, cleared by centrifugation at 14,000 x g for 30 min at 4° C. Protein extract was recovered and GST-HDP1-DBD protein was purified using Pierce GST Spin purification kit (Cat. N° 16106) following manufacturer directions. Protein of interest was dialyzed using Slide-A-Lyzer Dialysis Cassette 10,000 MWCO (ThermoScientific, Cat. N° 66810) and concentrated using Amicon Ultra Centrifugal filters 10,000 MWCO (Millipore, Cat. N° UFC901024). Purity was verified by Coomassie staining after SDS-PAGE and concentration was measured by Bradford assay.

Sequence encoding HDP1 aa2991-3078 were cloned into the MCS1 of the pRSFDuet-1 vector (Novagen) engineered with an N-terminal His-SUMO tag. The proteins were expressed in *E. coli* strain BL21 CodonPlus(DE3)-RIL (Stratagene). Bacteria were grown in Luria-Bertani medium at 37°C to OD600=0.8 and induced with 0.4 mM IPTG at 18°C overnight. Cells were collected via centrifugation at 5000xg and lysed via sonication in Lysis Buffer (20 mM Tris-HCl, pH 8.0, 500 mM NaCl, 20 mM imidazole, and 5% Glycerol) supplemented with 1 mM phenylmethylsulfonyl fluoride and 0.5% Triton X-100. Cellular debris was removed by centrifugation at 20,000xg, and the supernatant was loaded onto 5 ml HisTrap FF column (GE Healthcare) and eluted using the lysis buffer supplemented with 500 mM imidazole. The elution was dialyzed at 4°C overnight against the buffer (20 mM Tris-HCl, pH 8.0, 300 mM NaCl, 20 mM imidazole, and 5 mM β-mercaptoethanol) with ULP1 protease added (lab stock). The sample was reloaded on the HisTrap FF column to remove the His-SUMO tag. The flow-through was loaded on the Heparin

column (GE Healthcare) and eluted with a gradient of NaCl from 300 mM to 1 M. The target protein was further purified by size exclusion chromatography (Superdex 200 [16/60], GE Healthcare) in the buffer (20 mM Tris-HCl, pH 7.5, 200 mM NaCl, 1 mM MgCl₂, and 1 mM DTT). The high purity eluting fractions were detected by SDS-PAGE and concentrated to around 20 mg/ml. The protein was flash-frozen in liquid nitrogen and stored at -80°C.

Protein Binding Microarray

All GST-HDP1-DBD binding was analyzed twice in the PBMs. The PBM experiments were performed as previously described (Berger and Bulyk, 2009; Berger et al., 2006). Briefly, custom designed oligonucleotide arrays are double-stranded using a universal primer, incubated with GST-HDP1-DBD fusion proteins, visualized with Alexa-488 conjugated anti-GST antibody, and scanned using an Axon 4200A scanner. Proteins were used at the maximum concentration obtained from purification and represent one-fifth of the total reaction volume used on the PBM. In this study three different universal platforms were used covering all contiguous 8-mers as well as gapped 8-mers spanning up to 10 positions. After data normalization and calculation of enrichment scores the “Seed-and-Wobble” algorithm was applied to combine the data from two separate experiments and create position weight matrices (PWMs). An enrichment score cut-off of 0.45 was used to distinguish high affinity binding data from low affinity and non-specific binding. The score for each 8-mer reflects the affinity of a DNA binding domain for that sequence, with higher scores representing tighter interactions. Secondary motifs were identified by running the “rerank” program until E-scores below 0.45 were obtained. The PBM analysis suite was downloaded from the [_brain.bwh.harvard.edu/PBMANalysisSuite/index.html](http://brain.bwh.harvard.edu/PBMANalysisSuite/index.html).

Isothermal Titration Calorimetry

All the binding experiments were performed on a Microcal ITC 200 calorimeter. Purified HLH proteins were dialyzed overnight against the buffer (20 mM HEPES, pH 7.5, 150 mM NaCl, 1 mM DTT) at 4°C. DNA oligos were synthesized by Integrated DNA Technologies (IDT) and dissolved in the same buffer. The assays perform with 1 mM DNA duplexes containing the tandem motif (TAGTGACCTATGGTGCACTT) with 0.1 mM HLH90 proteins. Each reaction's exothermic heat was measured by sequential injection of the 2 µL DNA duplexes into proteins solution, spaced at intervals of 180 seconds. The titration was according to standard protocol at 20°C and the data were fitted using the program Origin 7.0.

Gel-shift Assays

Electrophoretic mobility shift assays were performed using Light Shift EMSA kits (Thermo Scientific) using 24 pg of protein and 40 fmol of probe, as previously described (Campbell et al., 2010). Biotinylated double-stranded probes were generated with the indicated sequence.

RNA Extraction, cDNA synthesis, and quantitative RT-PCR

Total RNA from saponin-lysed parasites was extracted using Trizol (Invitrogen) and Direct-Zol RNA MiniPrep Plus kit (Zymo Research). The cDNA was prepared from 100-500ng total RNA (pre-treated with 2U DNase I, amplification grade) using SuperScript III Reverse Transcriptase kit (Invitrogen) and random hexamers. Quantitative PCR was performed on the Quant Studio 6 Flex (Thermo Fisher) using iTaq Sybr Green (Bio-Rad) with specific primers for selected target genes (Table). Quantities were normalized to seryl-tRNA synthetase (PF3D7_0717700). Analysis of expression of the *var* gene family was performed by using the primer set described in Salanti et al. 2003 (Salanti et al., 2003).

RNA sequencing

Following gametocyte induction, highly synchronous cultures containing committed schizonts were added to fresh RBCs and allowed to reinvade for 12 hours prior to the addition of 50mM N-acetyl glucosamine to block the development of hemozoin-containing asexual trophozoites. On day 2 of gametocyte development, stage I gametocytes were purified magnetically and total RNA was extracted as described above. Following RNA isolation, total RNA integrity was checked using a 2100 Bioanalyzer (Agilent Technologies, Santa Clara, CA). RNA concentrations were measured using the NanoDrop system (Thermo Fisher Scientific, Inc., Waltham, MA). Preparation of RNA sample library and RNA-seq were performed by the Genomics Core Laboratory at Weill Cornell Medicine. rRNA was removed from Total RNA using Illumina Ribo Zero Gold for human/mouse/rat kit. Using Illumina TruSeq RNA Sample Library Preparation v2 kit (Illumina, San Diego, CA), Messenger RNA was fragmented into small pieces using divalent cations under elevated temperature. The cleaved RNA fragments were copied into first strand cDNA using reverse transcriptase and random primers. Second strand cDNA synthesis followed, using DNA Polymerase I and RNase H. The cDNA fragments then went through an end repair process, the addition of a single 'A' base, and then ligation of the adapters. The products were then purified and enriched with PCR to create the final cDNA library. were pooled and sequenced on Illumina HiSeq4000 sequencer with single-end 50 cycles. Read files were checked for quality by using FASTQC (<https://github.com/s-andrews/FastQC>). Reads were trimmed to remove low-quality

positions and adapter sequences using cutadapt (version 1.16) (Martin, 2011). Reads were mapped against the *P. falciparum* 3D7 reference genome v.40 (Warrenfeltz et al., 2018) using STAR aligner (version 2.61) (Dobin et al., 2012) and nuclear-encoded genes were analyzed for differential gene expression using cufflinks (version 2.2.1) (Trapnell et al., 2013). Genes with a false discovery rate of ≤ 0.05 with a mean FPKM > 5 in at least one strain were called significant. For genes with FPKM > 5 in one strain and no detectable expression in the other, FPKM values were set to 0.1 for purposes of fold-change calculation. Gene Set Enrichment Analysis was carried out with the FGSEA Bioconductor package (Korotkevich et al., 2019) with a false discovery cutoff of ≤ 0.05 .

Hi-C Sequencing

Parasites were crosslinked in 1.25% formaldehyde in warm PBS for 25 min on a rocking platform. Glycine was added to a final concentration of 150 mM, followed by 15 min of incubation at 37°C and 15 min of incubation at 4°C. The parasites were centrifuged at 660g for 20 min at 4°C, resuspended in 5 volumes of ice-cold PBS, and incubated for 10 min at 4°C. Parasites were centrifuged at 660g for 15 min at 4°C, washed once in ice-cold PBS, and stored as a pellet at -80°C. Parasite pellets were then thawed on ice in Hi-C lysis buffer (10 mM Tris-HCl at pH8.0, 10 mM NaCl, 2 mM AEBSF, Roche Complete Mini EDTA-free protease inhibitor cocktail, 0.25% Igepal CA-630). Parasite membranes were disrupted by passing the lysate through a 26.5-gauge needle 15 times with a syringe. Samples were spun and pellets were washed once with ice-cold Hi-C lysis buffer, resuspended in 0.5% SDS and incubated at 62°C for 10 min to solubilize the chromatin. The SDS was neutralized by the addition of nuclease-free water and 1% Triton X-100, for 15-minutes at 37°C. DNA was then digested using MboI restriction overnight at 37°C. After digestion, the enzyme was heat inactivated at 62°C for 20 min, and then cooled to RT. 5' overhangs were filled in by Biotin-14-dCTP (Invitrogen) using DNA Polymerase I and Large (Klenow) Fragment (NEB) for 45 min at 37°C. Blunt-end ligation was performed using T4 DNA Ligase at 20°C for 4 hours. The nuclei were spun down to remove random ligation products and to reduce the overall reaction volume and resuspend in decrosslinking buffer (50 mM Tris-HCl, pH 8.0, 1% SDS, 1 mM EDTA, 500 mM NaCl) before adding RNaseA (20 mg/ml) for 45 min at 37°C and proteinase K (NEB) treatment overnight at 45°C. DNA was extracted using Agencourt AMPure XP beads (Beckman Coulter) and eluted in 10 mM Tris-HCl at pH 8.0. The purified DNA was sheared on a Covaris S220 and biotinylated DNA fragments were pull-down using MyOne Streptavidin T1 magnetic beads (Invitrogen) at 55°C for 2 min, washed and resuspended in T4 DNA Ligase Buffer to perform end-repair on DNA fragments bound to the beads containing DNA

Polymerase I, Large (Klenow) Fragment (NEB), and T4 DNA Polymerase (NEB) and incubated for 30 min at 20°C. The beads were washed twice before performing A-tailing using Klenow Fragment (3'→5' exo-nuclease) (NEB) for 30 min at 37°C. The beads were then washed twice and resuspended in T4 DNA Ligase Buffer to perform adapter ligation using the NEBNext Illumina Adapter for 15 min at 20°C in a thermomixer. The beads were then resuspended in 100 µl of 10 mM Tris-HCl at pH 8.0 and transferred to a new tube to amplify the library using the HiFi HotStart ReadyMix (KAPA Biosystems) as well as the universal forward primer and barcoded reverse primer before being incubated with the following PCR program: 45 sec at 98°C, 12 cycles of 15 sec at 98°C, 30 sec at 55°C, 30 sec at 62°C and a final extension of 5 min at 62°C. The library was then purified using double-SPRI size selection, with 0.5Å~ right-side selection (25 µl AMPure XP beads) and 1.0Å~ left-side selection (25 µl AMPure XP beads). Libraries were quantified by NanoDrop (Thermo Scientific) and Bioanalyzer (Agilent), prior to multiplexing and sequencing in a 75-bp paired-end run on a NextSeq500 (Illumina).

Analysis of Hi-C Data

Bed files of virtual Mbol (GATC) digest of the *P. falciparum* genome were generated with digest_genome.py from the HiC-Pro suite (Servant et al., 2015). The paired-end reads were processed (i.e. mapped, paired, and de-duplicated), binned at 10kb resolution, and normalized using the ICE algorithm using HiC-Pro (Imakaev et al., 2012). Reproducibility and strain-dependent differences (Figure 6A) between Hi-C samples was evaluated by correlation analysis using HiCSpector (Yan et al., 2017) and GenomeDISCO (same correlation pattern as HiCSpector, not shown) (Ursu et al., 2018). Interaction maps (Figure S7) were generated by plotting intra-chromosomal ICE-normalized interactions. Summary statistics (Figure 6B) of intra-chromosomal interaction distances were calculated for each strain and chromosome from normalized ICE interaction counts using R. Differential interaction analysis was carried out at 10 kb resolution for each replicate using selfish (Ardakany et al., 2019) based on ICE-normalized interaction counts from the Hi-C Pro all-valid-pairs matrix and reformatted into the “.hic” file-format using Juicebox (Robinson et al., 2018). All genome-wide bin pairs with significant changes in interaction frequency between the *hdp1-ty1* and $\Delta hdp1$ strains with a FDR ≤ 0.1 in both replicate pairs are shown in the top left of Figure 6C. For the analysis of chromosome-end interactions, interactions fold-change were calculated for all interactions in bins between the chromosome end and the first protein coding gene. As the final bin on each chromosome varies in size, an additional bin was added for ends truncated by telomere healing (5R, 11R, and 14R) to ensure interaction counts were calculated for at least 10kb.

ACKNOWLEDGEMENTS

We wish to thank Dr. Pawan Malhotra for the generous gift of anti-Phil1 antibodies, V. Carruthers for the generous gift of anti-Ty1 antibodies, the Weill Cornell Medicine genomics core for technical support, M. Llinas and R. Bartfai for separate HDP1 ChIP-seq attempts with *hdp1-gfp* and *hdp1-ty1* gametocytes, respectively, as well as K. Deitsch and J. King for valuable feedback on the manuscript. This work was supported by startup funds from Weill Cornell Medicine (BK), NIAID 1R01AI141965 (BK), 1R01 AI125565 (ML), 1R01 AI136511 (KLR), R21 AI142506-01 (KLR), the University of California, Riverside (NIFA-Hatch-225935-KLR), and support from the Mathers Foundation (DJP).

AUTHOR CONTRIBUTIONS

Conceptualization: B.F.C.K.; Methodology: B.F.C.K., R.C.M., W.X., W.N., K.G.L.; Investigation: R.C.M., X.T., W.X., T.L., G.B., L.O., W.D.; Software, Formal Analysis, Data Curation: B.F.C.K., T.L.; Writing – Original Draft: R.C.M.; Writing – Review & Editing: B.F.C.K., R.C.M.; Visualization: R.C.M., B.F.C.K.; Supervision: B.F.C.K., K.G.L., M.L., W.N., D.P.; Project Administration: B.F.C.K.; Funding Acquisition: B.F.C.K.;

DECLARATIONS OF INTEREST

The authors declare no competing interests.

REFERENCES

- Ardakany, A.R., Ay, F., Lonardi, S., 2019. Selfish: discovery of differential chromatin interactions via a self-similarity measure. *Bioinformatics* 35, i145–i153. doi:10.1093/bioinformatics/btz362
- Balaji, S., Babu, M.M., Iyer, L.M., Aravind, L., 2005. Discovery of the principal specific transcription factors of Apicomplexa and their implication for the evolution of the AP2-integrase DNA binding domains. *Nucleic Acids Res* 33, 3994–4006. doi:10.1093/nar/gki709
- Bancells, C., Llorà-Batlle, O., Poran, A., Nötzel, C., Rovira-Graells, N., Elemento, O., Kafsack, B.F.C., Cortés, A., 2019. Revisiting the initial steps of sexual development in the malaria parasite *Plasmodium falciparum*. *Nat. Microbiol* 4, 144–154. doi:10.1038/s41564-018-0291-7
- Berger, M.F., Bulyk, M.L., 2009. Universal protein-binding microarrays for the comprehensive characterization of the DNA-binding specificities of transcription factors. *Nature Protocols* 4, 393–411. doi:10.1038/nprot.2008.195
- Berger, M.F., Philippakis, A.A., Qureshi, A.M., He, F.S., Estep, P.W., Bulyk, M.L., 2006. Compact, universal DNA microarrays to comprehensively determine transcription-factor binding site specificities. *Nat Biotechnol* 24, 1429–1435. doi:10.1038/nbt1246
- Bhattacharya, S., Conolly, R.B., Kaminski, N.E., Thomas, R.S., Andersen, M.E., Zhang, Q., 2010. A Bistable Switch Underlying B-Cell Differentiation and Its Disruption by the Environmental Contaminant 2,3,7,8-Tetrachlorodibenzo-p-dioxin. *Toxicol Sci* 115, 51–65. doi:10.1093/toxsci/kfq035
- Brancucci, N.M.B., Bertschi, N.L., Zhu, L., Niederwieser, I., Chin, W.H., Wampfler, R., Freymond, C., Rottmann, M., Felger, I., Bozdech, Z., Voss, T.S., 2014. Heterochromatin protein 1 secures survival and transmission of malaria parasites. *Cell Host Microbe* 16, 165–176. doi:10.1016/j.chom.2014.07.004
- Bunnik, E.M., Cook, K.B., Varoquaux, N., Batugedara, G., Prudhomme, J., Cort, A., Shi, L., Andolina, C., Ross, L.S., Brady, D., Fidock, D.A., Nosten, F., Tewari, R., Sinnis, P., Ay, F., Vert, J.-P., Noble, W.S., Le Roch, K.G., 2018. Changes in genome organization of parasite-specific gene families during the *Plasmodium* transmission stages. *Nature Communications* 9, 1910. doi:10.1038/s41467-018-04295-5
- Burgess, R.R., 1991. Use of polyethyleneimine in purification of DNA-binding proteins. *Meth. Enzymol.* 208, 3–10. doi:10.1016/0076-6879(91)08003-z
- Bürglin, T.R., Affolter, M., 2016. Homeodomain proteins: an update. *Chromosoma* 125, 497–521. doi:10.1007/s00412-015-0543-8
- Calhoun, S.F., Reed, J., Alexander, N., Mason, C.E., Deitsch, K.W., Kirkman, L.A., Boyle, J.P., 2017. Chromosome End Repair and Genome Stability in *Plasmodium falciparum*. *mBio* 8, e00547–17. doi:10.1128/mBio.00547-17
- Campbell, T.L., De Silva, E.K., Olszewski, K.L., Elemento, O., Llinás, M., 2010. Identification and genome-wide prediction of DNA binding specificities for the ApiAP2 family of regulators from the malaria parasite. *PLoS Pathog* 6, e1001165. doi:10.1371/journal.ppat.1001165
- Coleman, B.I., Skillman, K.M., Jiang, R.H.Y., Childs, L.M., Altenhofen, L.M., Ganter, M., Leung, Y., Goldowitz, I., Kafsack, B.F.C., Marti, M., Llinás, M., Buckee, C.O., Duraisingh, M.T., 2014. A *Plasmodium falciparum* Histone Deacetylase Regulates Antigenic Variation and Gametocyte Conversion. *Cell Host Microbe* 16, 177–186. doi:10.1016/j.chom.2014.06.014

Dobin, A., Davis, C.A., Schlesinger, F., Drenkow, J., Zaleski, C., Jha, S., Batut, P., Chaisson, M., Gingeras, T.R., 2012. STAR: ultrafast universal RNA-seq aligner. *Bioinformatics* 29, 15–21. doi:10.1093/bioinformatics/bts635

Filarsky, M., Fraschka, S.A., Niederwieser, I., Brancucci, N.M.B., Carrington, E., Carrió, E., Moes, S., Jenoe, P., Bartfai, R., Voss, T.S., 2018. GDV1 induces sexual commitment of malaria parasites by antagonizing HP1-dependent gene silencing. *Science* 359, 1259–1263. doi:10.1126/science.aan6042

Flueck, C., Bartfai, R., Niederwieser, I., Witmer, K., Alako, B.T.F., Moes, S., Bozdech, Z., Jenoe, P., Stunnenberg, H.G., Voss, T.S., 2010. A major role for the *Plasmodium falciparum* ApiAP2 protein PfSIP2 in chromosome end biology. *PLoS Pathog* 6, e1000784. doi:10.1371/journal.ppat.1000784

Flueck, C., Bartfai, R., Volz, J., Niederwieser, I., Salcedo-Amaya, A.M., Alako, B.T.F., Ehlgen, F., Ralph, S.A., Cowman, A.F., Bozdech, Z., Stunnenberg, H.G., Voss, T.S., 2009. *Plasmodium falciparum* Heterochromatin Protein 1 Marks Genomic Loci Linked to Phenotypic Variation of Exported Virulence Factors. *PLoS Pathog* 5, e1000569. doi:10.1371/journal.ppat.1000569

Fraschka, S.A., Filarsky, M., Hoo, R., Niederwieser, I., Yam, X.Y., Brancucci, N.M.B., Mohring, F., Mushunje, A.T., Huang, X., Christensen, P.R., Nosten, F., Bozdech, Z., Russell, B., Moon, R.W., Marti, M., Preiser, P.R., Bartfai, R., Voss, T.S., 2018. Comparative Heterochromatin Profiling Reveals Conserved and Unique Epigenome Signatures Linked to Adaptation and Development of Malaria Parasites. *Cell Host Microbe* 23, 407–420.e8. doi:10.1016/j.chom.2018.01.008

Ghorbal, M., Gorman, M., Macpherson, C.R., Martins, R.M., Scherf, A., Lopez-Rubio, J.J., 2014. Genome editing in the human malaria parasite *Plasmodium falciparum* using the CRISPR-Cas9 system. *Nat Biotechnol* 32, 819–821. doi:10.1038/nbt.2925

Hedgethorpe, K., Eustermann, S., Yang, J.-C., Ogden, T.E.H., Neuhaus, D., Bloomfield, G., 2017. Homeodomain-like DNA binding proteins control the haploid-to-diploid transition in *Dictyostelium*. *Science advances* 3, e1602937. doi:10.1126/sciadv.1602937

Imakaev, M., Fudenberg, G., McCord, R.P., Naumova, N., Goloborodko, A., Lajoie, B.R., Dekker, J., Mirny, L.A., 2012. Iterative correction of Hi-C data reveals hallmarks of chromosome organization. *Nat Meth* 9, 999–1003. doi:10.1038/nmeth.2148

Josling, G.A., Russell, T.J., Venezia, J., Orchard, L., van Biljon, R., Painter, H.J., Llinás, M., 2020. Dissecting the role of PfAP2-G in malaria gametocytogenesis. *Nature Communications* 11, 1–13. doi:10.1038/s41467-020-15026-0

Kafsack, B.F.C., Rovira-Graells, N., Clark, T.G., Bancells, C., Crowley, V.M., Campino, S.G., Williams, A.E., Drought, L.G., Kwiatkowski, D.P., Baker, D.A., Cortés, A., Llinás, M., 2014. A transcriptional switch underlies commitment to sexual development in malaria parasites. *Nature* 507, 248–252. doi:10.1038/nature12920

Kent, R.S., Modrzynska, K.K., Cameron, R., Philip, N., Billker, O., Waters, A.P., 2018. Inducible developmental reprogramming redefines commitment to sexual development in the malaria parasite *Plasmodium berghei*. *Nat. Microbiol* 3, 1206–1213. doi:10.1038/s41564-018-0223-6

Korotkevich, G., Sukhov, V., Sergushichev, A., 2019. Fast gene set enrichment analysis. *bioRxiv* 10, 060012. doi:10.1101/060012

Lopez-Rubio, J.J., Mancio-Silva, L., Scherf, A., 2009. Genome-wide analysis of heterochromatin associates clonally variant gene regulation with perinuclear repressive centers in malaria parasites. *Cell Host Microbe* 5, 179–190. doi:10.1016/j.chom.2008.12.012

Martin, M., 2011. Cutadapt removes adapter sequences from high-throughput sequencing reads. *EMBnet.journal* 17, 10–12.

Mehnert, A.-K., Simon, C.S., Guizetti, J., 2019. Immunofluorescence staining protocol for STED nanoscopy of Plasmodium-infected red blood cells. *Mol Biochem Parasitol* 229, 47–52. doi:10.1016/j.molbiopara.2019.02.007

Modrzynska, K., Pfander, C., Chappell, L., Yu, L., Suarez, C., Dundas, K., Gomes, A.R., Goulding, D., Rayner, J.C., Choudhary, J., Billker, O., 2017. A Knockout Screen of ApiAP2 Genes Reveals Networks of Interacting Transcriptional Regulators Controlling the Plasmodium Life Cycle. *Cell Host Microbe* 21, 11–22. doi:10.1016/j.chom.2016.12.003

Moll, K., Ljungström, I., Perlmann, H., Scherf, A., 2008. *Methods in malaria research*. Manassas.

Morlon-Guyot, J., Hajj, El, H., Martin, K., Fois, A., Carrillo, A., Berry, L., Burchmore, R., Meissner, M., Lebrun, M., Daher, W., 2018. A proteomic analysis unravels novel CORVET and HOPS proteins involved in Toxoplasma gondii secretory organelles biogenesis. *Cell Microbiol* 20, e12870. doi:10.1111/cmi.12870

Nixon, C.P., Nixon, C.E., Michelow, I.C., Silva-Viera, R.A., Colantuono, B., Obeidallah, A.S., Jha, A., Dockery, D., Raj, D., Park, S., Duffy, P.E., Kurtis, J.D., 2018. Antibodies to PfsEGXP, an Early Gametocyte-Enriched Phosphoprotein, Predict Decreased Plasmodium falciparum Gametocyte Density in Humans. *J INFECT DIS* 218, 1792–1801. doi:10.1093/infdis/jiy416

Norman, T.M., Lord, N.D., Paulsson, J., Losick, R., 2015. Stochastic Switching of Cell Fate in Microbes. *Annu Rev Microbiol* 69, 381–403. doi:10.1146/annurev-micro-091213-112852

Painter, H.J., Carrasquilla, M., Llinás, M., 2017. Capturing in vivo RNA transcriptional dynamics from the malaria parasite Plasmodium falciparum. *Genome Res* 27, 1074–1086. doi:10.1101/gr.217356.116

Park, B.O., Ahrends, R., Teruel, M.N., 2012. Consecutive Positive Feedback Loops Create a Bistable Switch that Controls Preadipocyte-to-Adipocyte Conversion. *Cell Reports* 2, 976–990. doi:10.1016/j.celrep.2012.08.038

Parkyn Schneider, M., Liu, B., Glock, P., Suttie, A., McHugh, E., Andrew, D., Batinovic, S., Williamson, N., Hanssen, E., McMillan, P., Hliscs, M., Tilley, L., Dixon, M.W.A., 2017. Disrupting assembly of the inner membrane complex blocks Plasmodium falciparum sexual stage development. *PLoS Pathog* 13, e1006659. doi:10.1371/journal.ppat.1006659

Poran, A., Nötzel, C., Aly, O., Mencia-Trinchant, N., Harris, C.T., Guzman, M.L., Hassane, D.C., Elemento, O., Kafack, B.F.C., 2017. Single-cell RNA sequencing reveals a signature of sexual commitment in malaria parasites. *Nature* 551, 95–99. doi:10.1038/nature24280

Pradhan, L., Genis, C., Scone, P., Weinberg, E.O., Kasahara, H., Nam, H.-J., 2012. Crystal Structure of the Human NKX2.5 Homeodomain in Complex with DNA Target. *Biochemistry* 51, 6312–6319. doi:10.1021/bi300849c

Prommana, P., Uthapibull, C., Wongsombat, C., Kamchonwongpaisan, S., Yuthavong, Y., Knuepfer, E., Holder, A.A., Shaw, P.J., 2013. Inducible Knockdown of Plasmodium Gene Expression Using the glmS Ribozyme. *PLoS ONE* 8, e73783. doi:10.1371/journal.pone.0073783

Robinson, J.T., Turner, D., Durand, N.C., Thorvaldsdóttir, H., Mesirov, J.P., Aiden, E.L., 2018. Juicebox.js Provides a Cloud-Based Visualization System for Hi-C Data. *Cels* 6, 256–258.e1. doi:10.1016/j.cels.2018.01.001

- Rug, M., Maier, A.G., 2012. Transfection of Plasmodium falciparum, in: Malaria, Methods in Molecular Biology. Humana Press, Totowa, NJ, Totowa, NJ, pp. 75–98. Doi:10.1007/978-1-62703-026-7_6
- Saini, E., Zeeshan, M., Brady, D., Pandey, R., Kaiser, G., Koreny, L., Kumar, P., Thakur, V., Tatiya, S., Katris, N.J., Limenitakis, R.S., Kaur, I., Green, J.L., Bottrill, A.R., Guttery, D.S., Waller, R.F., Heussler, V., Holder, A.A., Mohammed, A., Malhotra, P., Tewari, R., 2017. Ph otosensitized I NA- L abelled protein 1 (PhIL1) is novel component of the inner membrane complex and is required for Plasmodium parasite development. Sci. Rep. 7, 15577. Doi:10.1038/s41598-017-15781-z
- Salanti, A., Staalsoe, T., Lavstsen, T., Jensen, A.T.R., Sowa, M.P.K., Arnot, D.E., Hviid, L., Theander, T.G., 2003. Selective upregulation of a single distinctly structured var gene in chondroitin sulphate A- adhering Plasmodium falciparum involved in pregnancy-associated malaria. Mol Microbiol 49, 179–191. Doi:10.1046/j.1365-2958.2003.03570.x
- Satory, D., Gordon, A.J., Halliday, J.A., Herman, C., 2011. Epigenetic switches: can infidelity govern fate in microbes? Curr Opin Microbiol 14, 212–217. Doi:10.1016/j.mib.2010.12.004
- Servant, N., Varoquaux, N., Lajoie, B.R., Viara, E., Chen, C.-J., Vert, J.-P., Heard, E., Dekker, J., Barillot, E., 2015. HiC-Pro: an optimized and flexible pipeline for Hi-C data processing. Genome Biol 16, 1–11. Doi:10.1186/s13059-015-0831-x
- Sinha, A., Hughes, K.R., Modrzynska, K.K., Otto, T.D., Pfander, C., Dickens, N.J., Religa, A.A., Bushell, E., Graham, A.L., Cameron, R., Kafack, B.F.C., Williams, A.E., Llinás, M., Berriman, M., Billker, O., Waters, A.P., 2014. A cascade of DNA-binding proteins for sexual commitment and development in Plasmodium. Nature 507, 253–257. Doi:10.1038/nature12970
- Tanaka, T.Q., Williamson, K.C., 2011. A malaria gametocytocidal assay using oxidoreduction indicator, alamarBlue. Mol Biochem Parasitol 177, 160–163. Doi:10.1016/j.molbiopara.2011.02.005
- Tibúrcio, M., Silvestrini, F., Bertuccini, L., Sander, A.F., Turner, L., Lavstsen, T., Alano, P., 2013. Early gametocytes of the malaria parasite Plasmodium falciparum specifically remodel the adhesive properties of infected erythrocyte surface. Cell Microbiol 15, 647–659. Doi:10.1111/cmi.12062
- Trapnell, C., Hendrickson, D.G., Sauvageau, M., Goff, L., Rinn, J.L., Pachter, L., 2013. Differential analysis of gene regulation at transcript resolution with RNA-seq. Nat Biotechnol 31, 46–53. Doi:10.1038/nbt.2450
- Ursu, O., Boley, N., Taranova, M., Wang, Y.X.R., Yardimci, G.G., Stafford Noble, W., Kundaje, A., 2018. GenomeDISCO: a concordance score for chromosome conformation capture experiments using random walks on contact map graphs. Bioinformatics 34, 2701–2707. Doi:10.1093/bioinformatics/bty164
- van Biljon, R., van Wyk, R., Painter, H.J., Orchard, L., Reader, J., Niemand, J., Llinás, M., Birkholtz, L.- M., 2019. Hierarchical transcriptional control regulates Plasmodium falciparum sexual differentiation. BMC Genomics 20, 920. Doi:10.1186/s12864-019-6322-9
- Warrenfeltz, S., Basenko, E.Y., Crouch, K., Harb, O.S., Kissinger, J.C., Roos, D.S., Shanmugasundram, A., Silva-Franco, F., 2018. EuPathDB: The Eukaryotic Pathogen Genomics Database Resource. Methods Mol Biol 1757, 69–113. Doi:10.1007/978-1-4939-7737-6_5
- Yan, K.-K., Yardimci, G.G., Yan, C., Noble, W.S., Gerstein, M., 2017. HiC-spector: a matrix library for spectral and reproducibility analysis of Hi-C contact maps. Bioinformatics 33, 2199–2201. doi:10.1093/bioinformatics/btx152

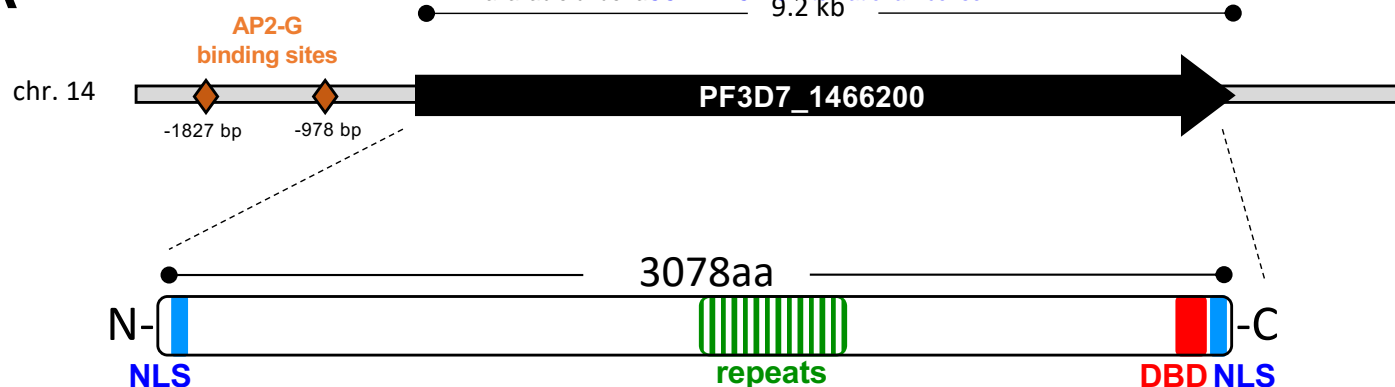
Young, J.A., Fivelman, Q.L., Blair, P.L., la Vega, de, P., Le Roch, K.G., Zhou, Y., Carucci, D.J., Baker, D.A., Winzeler, E.A., 2005. The *Plasmodium falciparum* sexual development transcriptome: a microarray analysis using ontology-based pattern identification. *Mol Biochem Parasitol* 143, 67–79. doi:10.1016/j.molbiopara.2005.05.007

Yuda, M., Iwanaga, S., Kaneko, I., Kato, T., 2015. Global transcriptional repression: An initial and essential step for *Plasmodium* sexual development. *Proceedings of the National Academy of Sciences*. doi:10.1073/pnas.1504389112

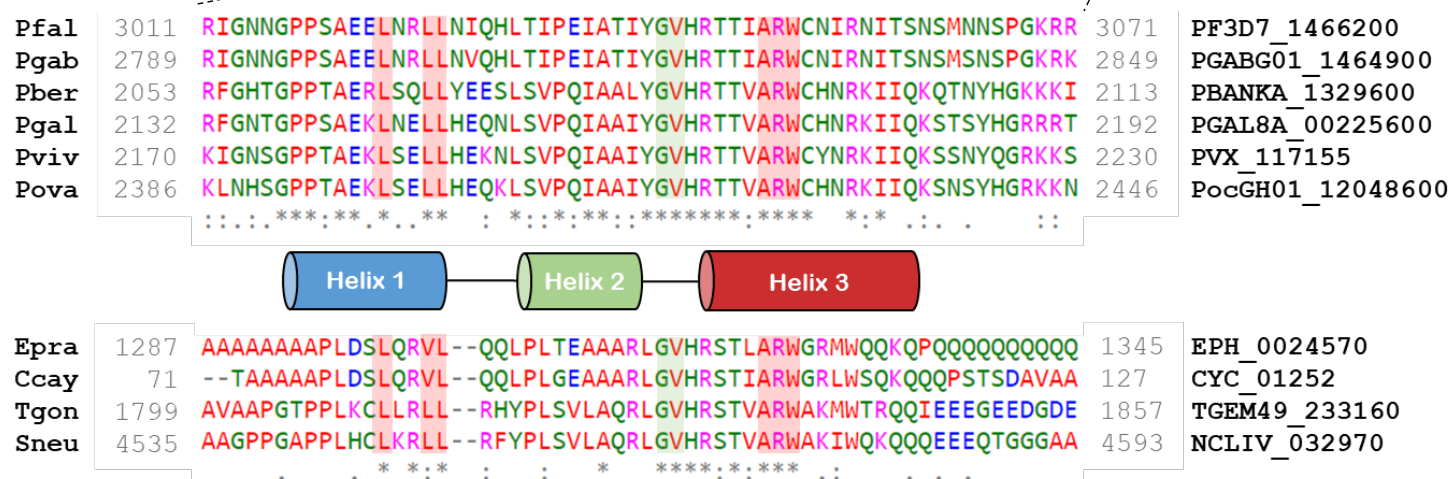
Yuda, M., Kaneko, I., Iwanaga, S., Mura, Y., Kato, T., 2019. Female-specific gene regulation in malaria parasites by an AP2-family transcription factor. *Mol Microbiol* 6, 1–51. doi:10.1111/mmi.14334

Zhang, C., Li, Z., Cui, H., Jiang, Y., Yang, Z., Wang, X., Gao, H., Liu, C., Zhang, S., Su, X.-Z., Yuan, J., 2017. Systematic CRISPR-Cas9-Mediated Modifications of *Plasmodium yoelii* ApiAP2 Genes Reveal Functional Insights into Parasite Development. *mBio* 8, 610. doi:10.1128/mBio.01986-17

A



B



C

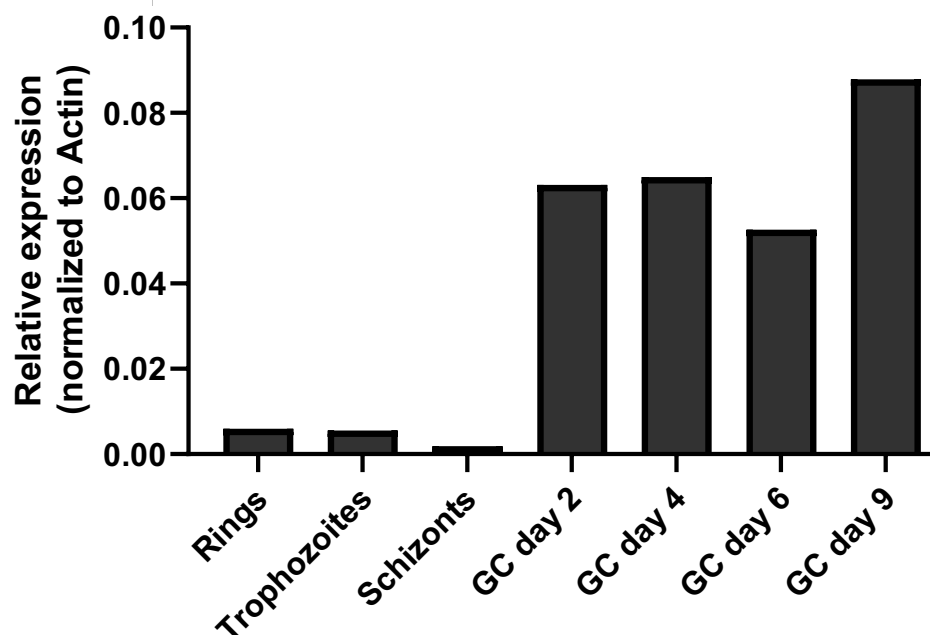


Figure 1: The predicted DNA-binding protein HDP1 is expressed in gametocytes. (A) The single exon locus Pf3D7_1466200 encodes a large 3078aa protein with a predicted C-terminal Helix-Turn-Helix DNA-binding domain (DBD) and two nuclear localization signals (NLS). Multiple AP2-G binding sites are located in the 2kb promoter region. (B) Alignment of the helix-turn-helix domain for homologs from other apicomplexan parasites. (C) Quantitative RT-PCR of *hdp1* transcripts found minimal expression in asexual blood stages with upregulation during gametocyte development. (mean of n=2).

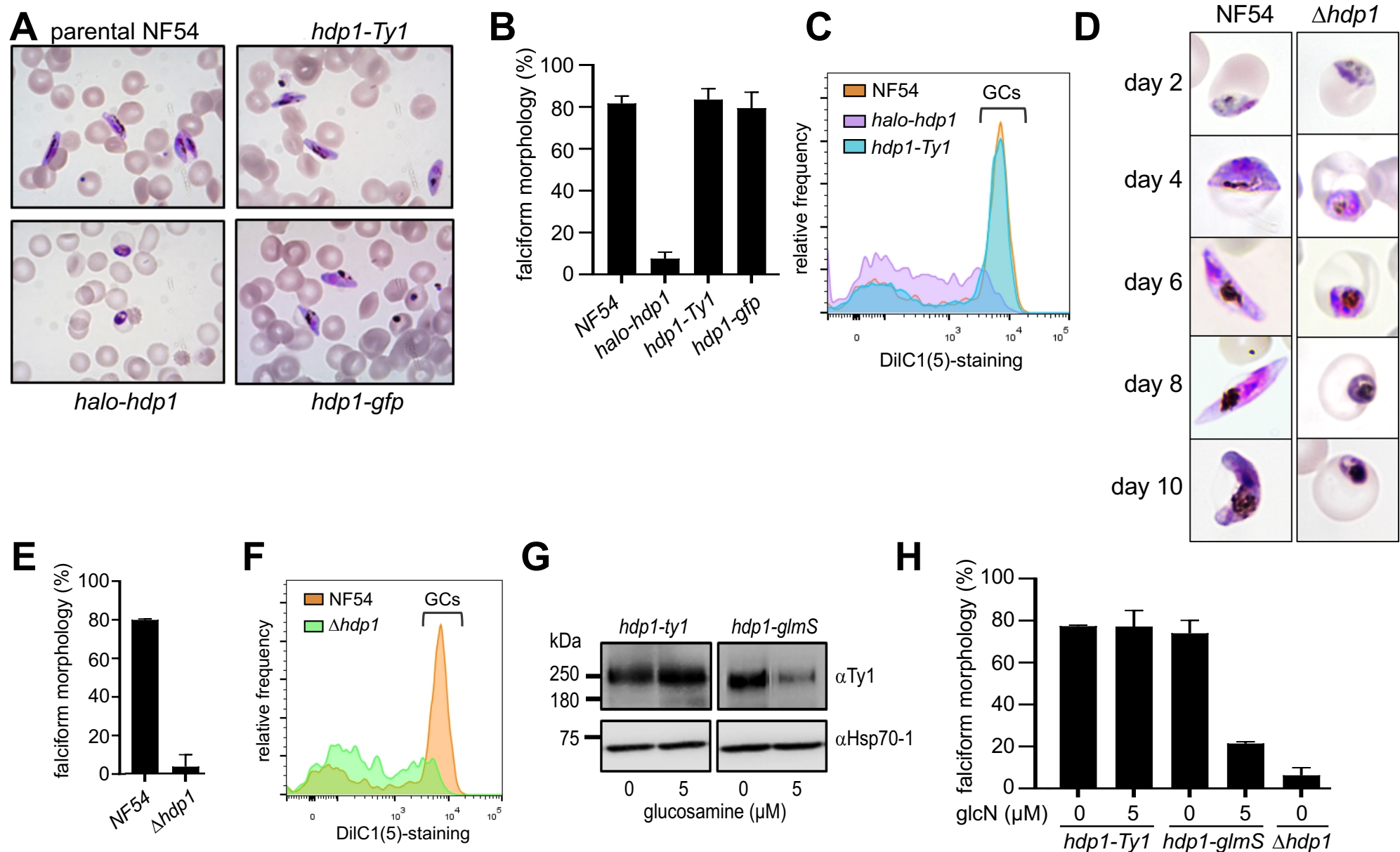


Figure 2: Loss of PfHDP1 function disrupts gametocyte maturation. (A-C) N-terminal tagging of the endogenously encoded HDP1 (*halo-hdp1*) blocked maturation of gametocytes (GCs) while C-terminal tagging of the endogenous locus with either GFP (*hdp1-gfp*) or a triple Ty1 (*hdp1-ty1x3*) epitope had no effect on gametocyte morphology or viability, as determined by membrane potential staining with DiIC(1)-5 on day 5 of gametocyte maturation. (D-F) Targeted disruption of the *hdp1* locus ($\Delta hdp1$) similarly blocked gametocyte maturation. Bar graphs show mean \pm s.e.m. of n=3 (G) Glucosamine-inducible knockdown of HDP1 in *hdp1-Ty1* and *hdp1-glmS* day 5 gametocytes. Representative of n=3. (H) Percentage of falciform day 5 gametocytes in response to 5 mM glucosamine (GlcN). Images and flow cytometry plots are representative of n=3.

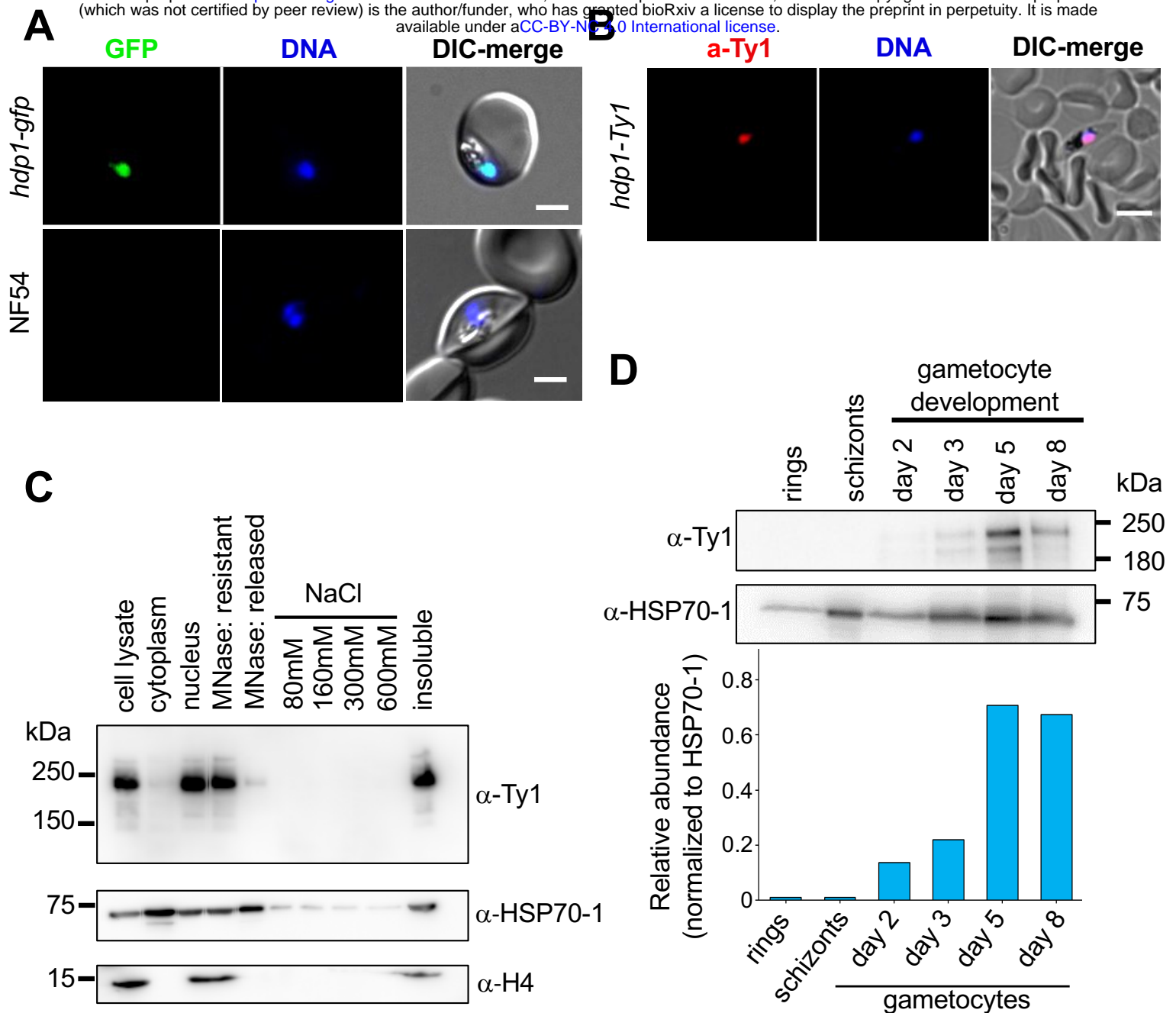


Figure 3: PfHDP1 localizes to the nucleus of gametocytes. (A) Live-cell fluorescence microscopy of *hdp1-gfp* and parental NF54 gametocytes on day 5 of maturation stained with the DNA dye Hoechst33342 (blue). Scale Bar: 2µm. Representative of n=2. (B) Immunofluorescence microscopy of *hdp1-ty1x3* and parental NF54 gametocytes on day 5 of maturation co-stained with anti-ty1 antibodies (red) and Hoechst33342 (blue). Scale Bar: 5µm. Representative of n=2. (C) Western blot of cytoplasmic and nuclear extracts of *hdp1-ty1x3* gametocytes on day 5 of maturation with stained with antibodies against the ty1 epitope tag, the histone H4, and HSP70-1. Representative of n=3. (D) Western blotting of parasite lysates in asexual stages and during gametocyte maturation shows HDP1 is expressed during the stages of gametocytogenesis. Representative of n=3.

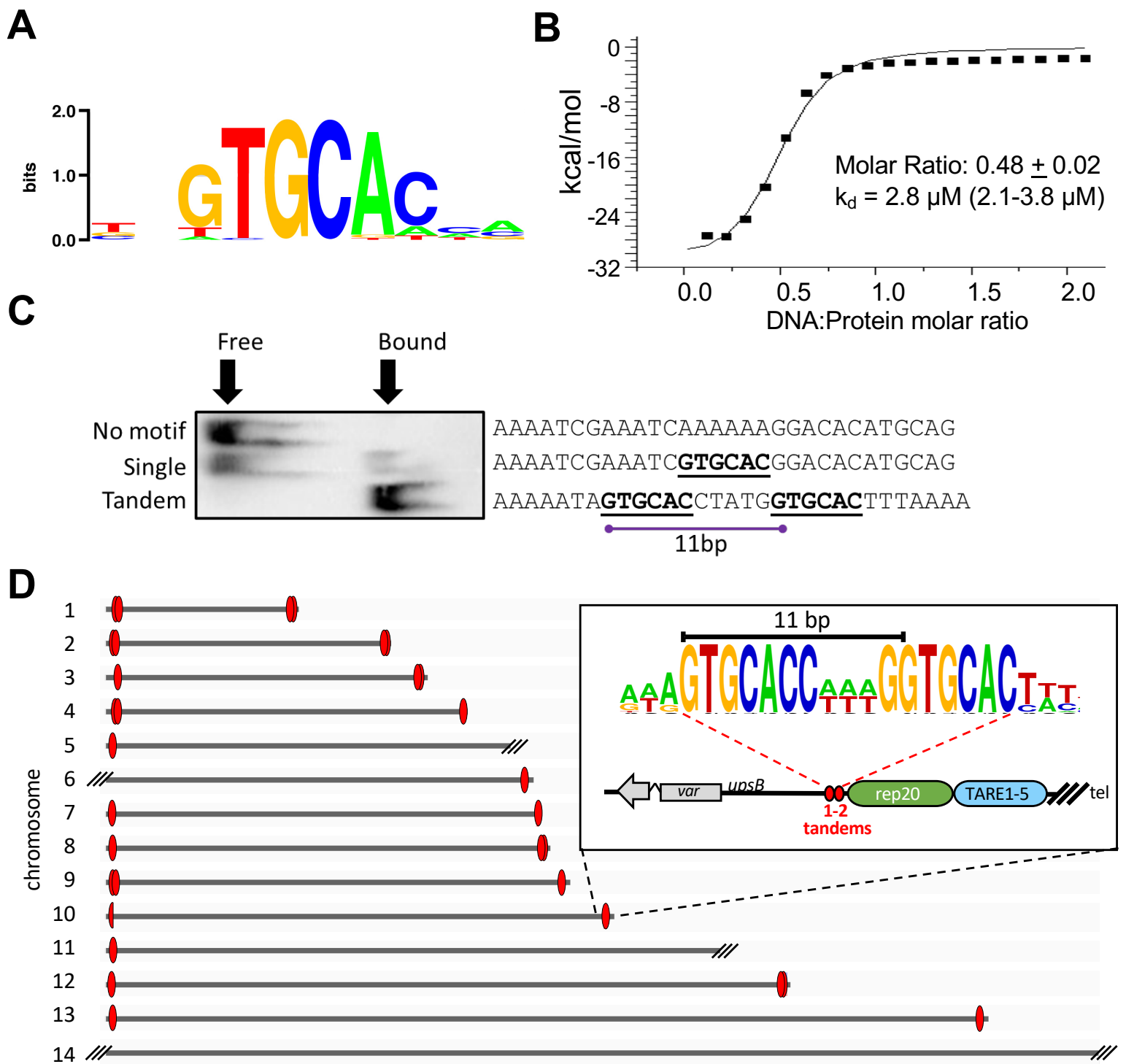


Figure 4: The HDP1 HTH domain dimers recognize a tandem GC-rich motif found at chromosome ends. (A) Maximum enrichment DNA motif for for the GST-HDP1 HTH domain from a protein-binding microarray. **(B)** Isothermal calorimetry indicates the HDP1-HTH domain recognizes DNA as a dimer. $n=2$. **(C)** Optimal gel-shift was observed for probes containing a tandem motif with a 5bp spacer compared to probes with either a single or no motif. Representative of $n=3$. **(D)** Tandem HDP1 motifs with a 5-6bp spacer occur exclusively in arrays of 1-2 copies within either 7 bp or 28 bp of the last *rep20* sub-telomeric repeats at all full-length chromosome ends. The motif on the left end of chromosome 10 is degenerate but its positioning is conserved. Truncation by telomere healing resulted in the loss of *rep20* adjacent region at five other chromosome ends.

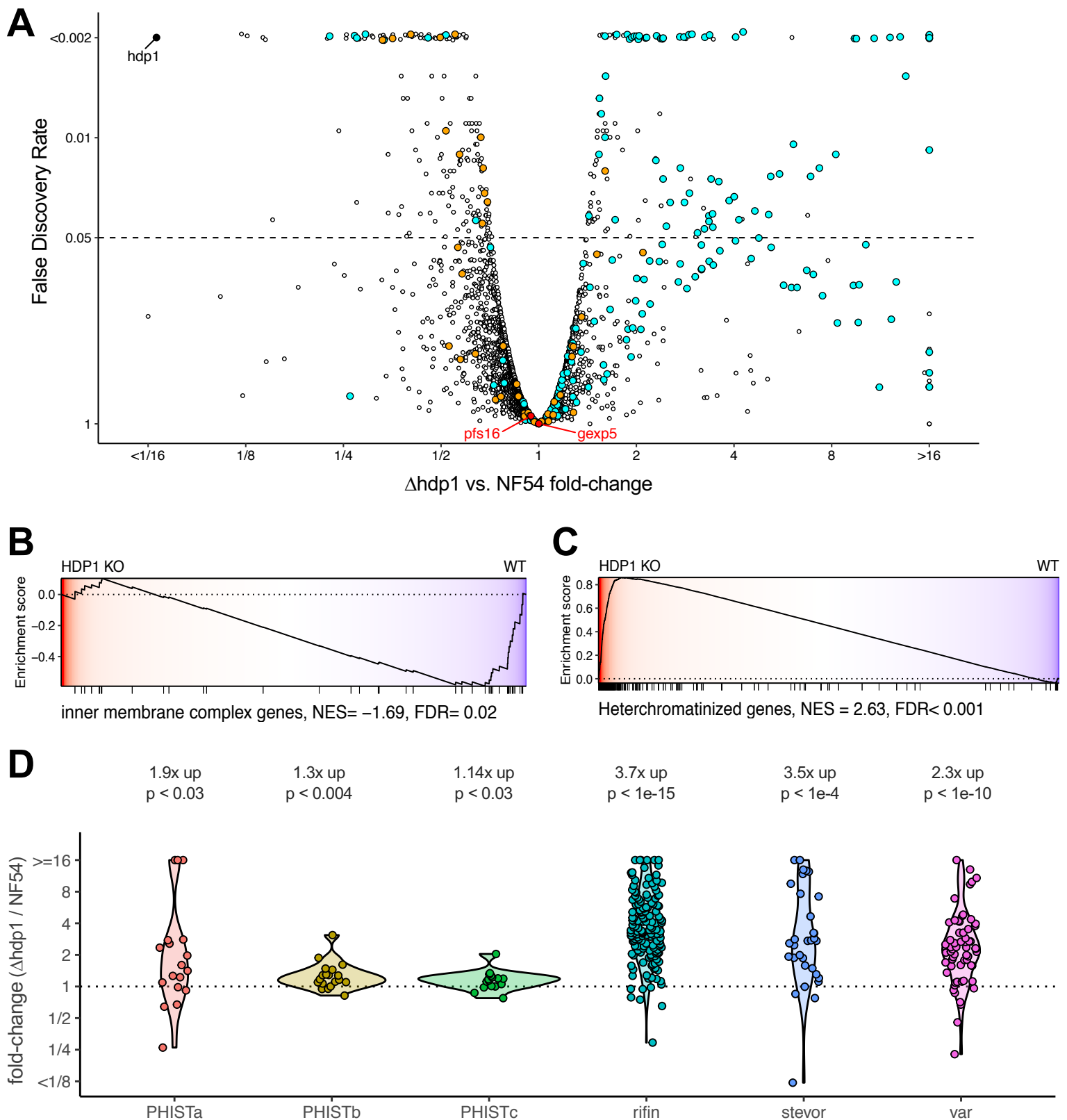


Figure 5: Disruption of HDP1 results in leaky expression of heterochromatin-associated genes and reduced expression of inner membrane complex genes in early gametocytes. **(A)** Genome-wide comparison of differential gene expression in $\Delta hdp1$ and parental NF54 gametocytes on day 2 of gametocytogenesis (stage I, $n=2$). *hdp1* (solid black), heterochromatin-associated genes (cyan), IMC genes (orange) and the two canonical early gametocyte markers, *pfs16* and *gexp5* (red) are highlighted. Gene set enrichment analysis (GSEA) indicated significant downregulation of IMC genes **(B)** and global upregulation of heterochromatin associated genes **(C)**. **(D)** Heterochromatin associated gene families with significant up regulation in $\Delta hdp1$. Geometric mean fold-changes and p-values (two-sided, one sample t-test) are indicated.

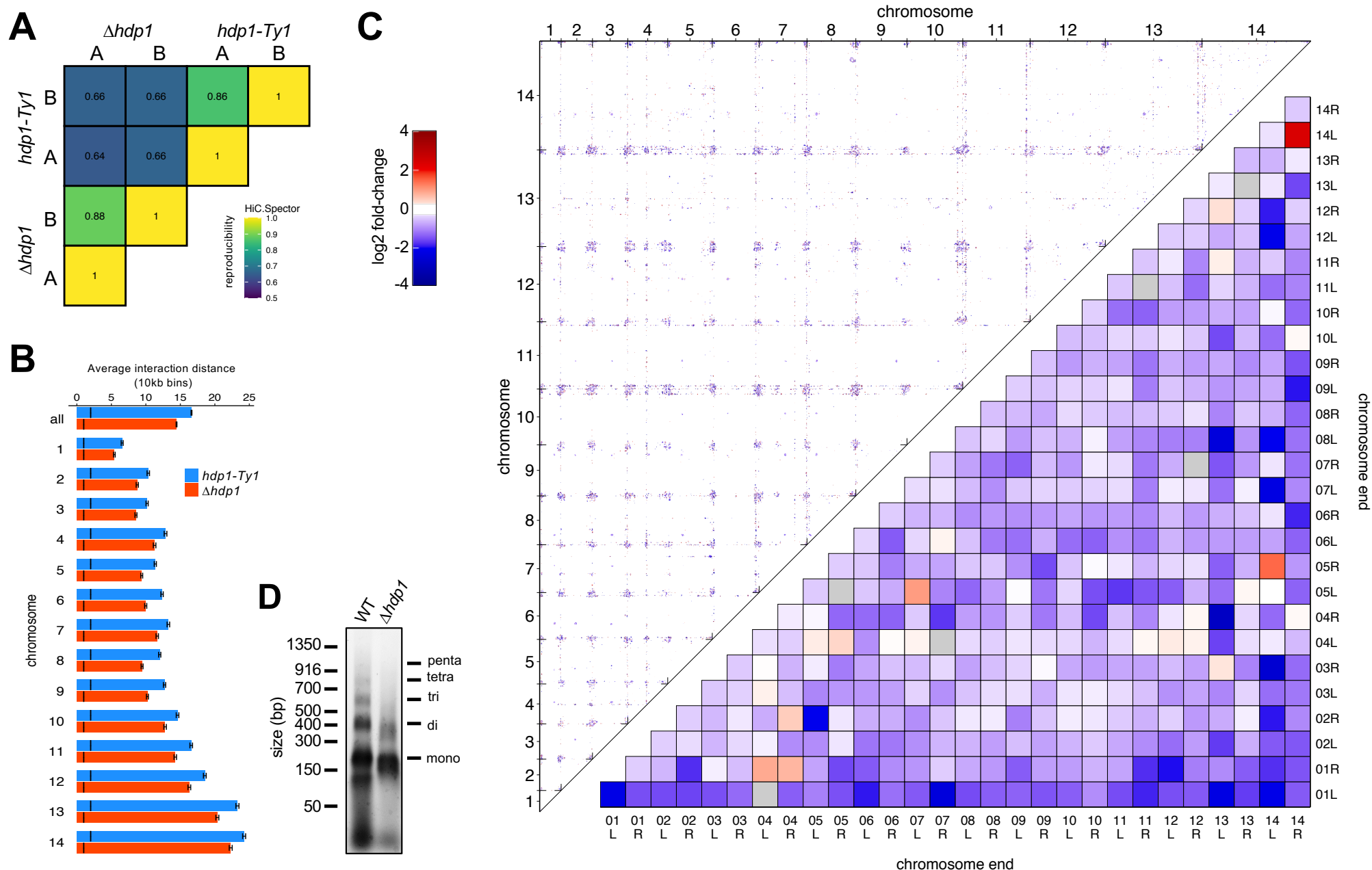


Figure 6: Loss of HDP1 results in reduced telomere clustering. (A) Analysis of Hi-C interaction maps for each sample by HiC.Spector highlights reproducibility of replicates and illustrate systematic differences between the strains. Scale ranges from 0-1.0 but only 0.6-1.0 is shown for improved visibility. **(B)** Mean HiC interaction distance in $hdp1-Ty1$ (blue) and $\Delta hdp1$ (red) stage I gametocytes. Error-bars indicate the 95% confidence interval and the black line indicates the median interaction distance. **(C)** Top triangle shows significant genome-wide changes in the $\Delta hdp1$ compared to $hdp1-Ty1$ with inside ticks indicating chromosome boundaries. FDR < 0.1. The average interaction fold-changes for all pair-wise interactions of chromosome ends are shown in the bottom triangle. **(D)** Accelerated MNase digestion of $\Delta hdp1$ chromatin from stage I gametocytes indicates reduced chromatin compaction.

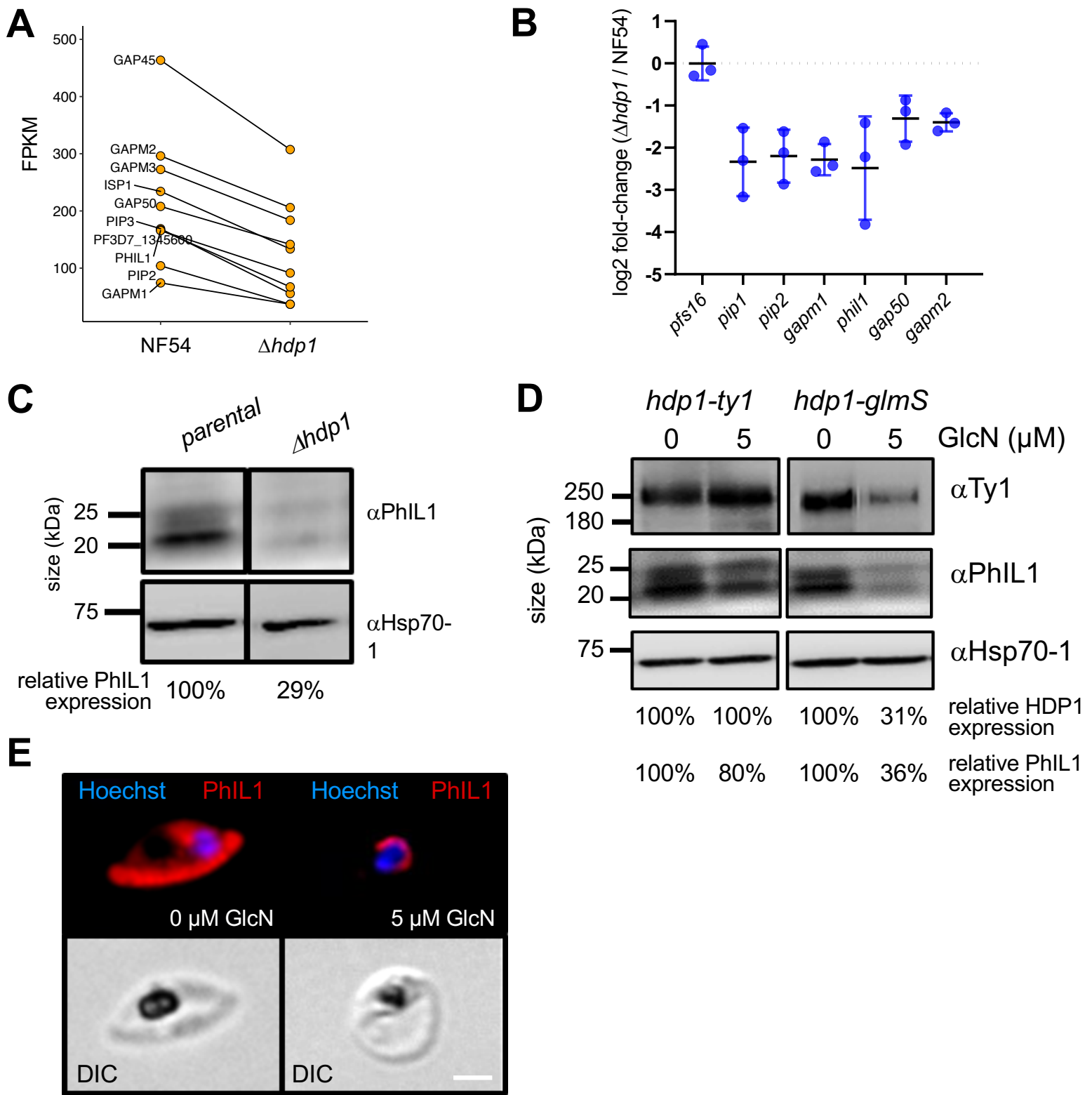


Figure 7: HDP1 regulates PhIL1-dependent expansion of the inner membrane complex in early gametocytes. (A) Transcripts encoding inner membrane complex proteins are down-regulated in $\Delta hdp1$ day 2 gametocytes. Normalized transcript levels (FPKM) in NF54 and $\Delta hdp1$ day 2 gametocytes. (B) Validation of down-regulation by qRT-PCR. Levels of the canonical early gametocyte marker *pfs16* remained unchanged. (n=3) (C) PhIL1 protein levels in parental and $\Delta hdp1$ day 5 gametocytes. Hsp70-1 abundance shown as the loading control. Representative result of n=2. (D) Day 5 morphology of *hdp1-ty1* and *hdp1-glmS* gametocytes under 0 and 5 μM glucosamine. HDP1 and PhIL1 protein levels in *hdp1-ty1* and $\Delta hdp1$ day 5 gametocytes. Hsp70-1 abundance shown as the loading control. Representative result of n=3. (E) Immunofluorescence microscopy of PhIL1 distribution in day 5 gametocytes of *hdp1-glmS* under 0 and 5 μM glucosamine. Scale Bar: 3μm

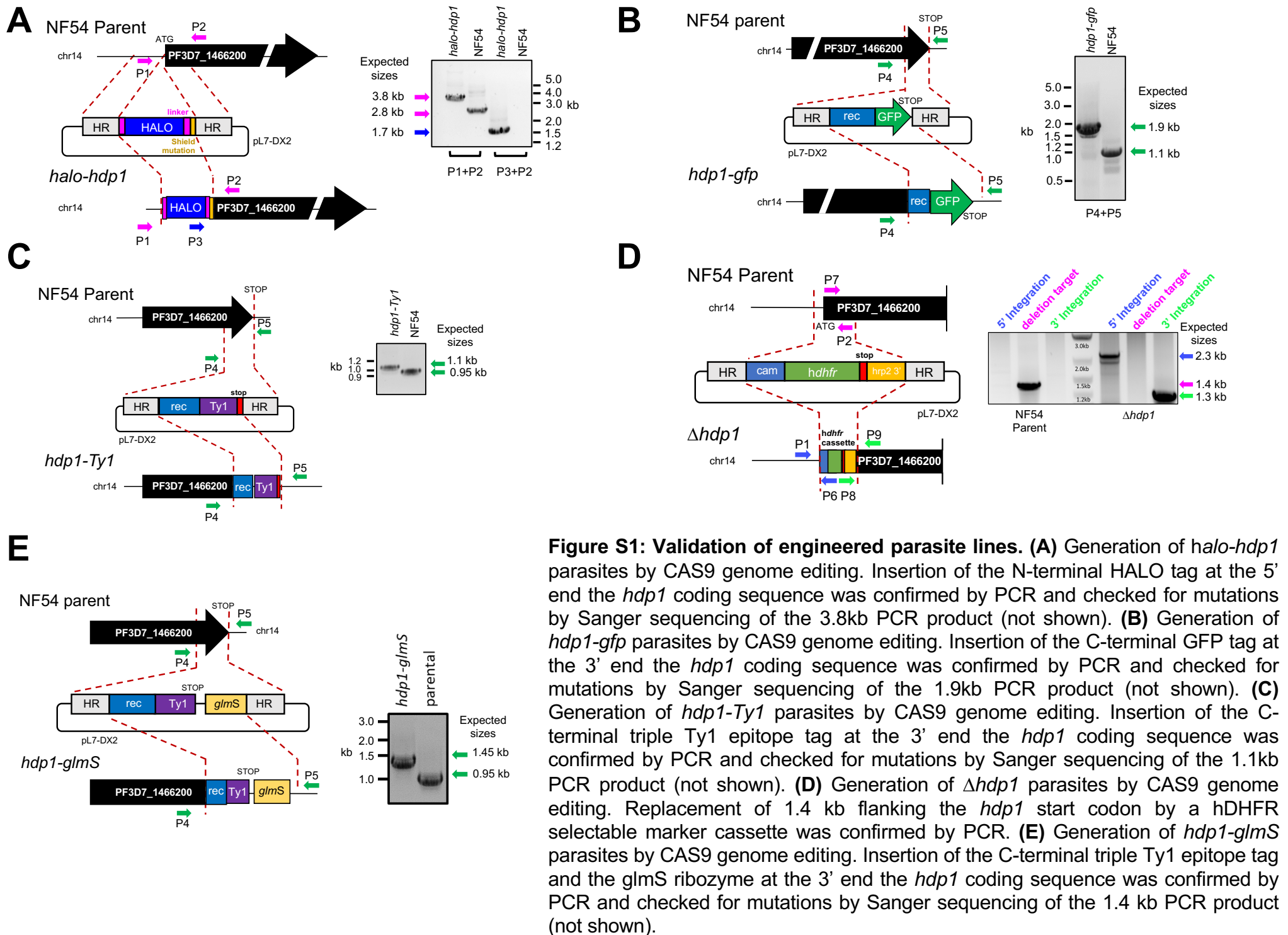


Figure S1: Validation of engineered parasite lines. (A) Generation of *halo-hdp1* parasites by CAS9 genome editing. Insertion of the N-terminal HALO tag at the 5' end the *hdp1* coding sequence was confirmed by PCR and checked for mutations by Sanger sequencing of the 3.8kb PCR product (not shown). (B) Generation of *hdp1-gfp* parasites by CAS9 genome editing. Insertion of the C-terminal GFP tag at the 3' end the *hdp1* coding sequence was confirmed by PCR and checked for mutations by Sanger sequencing of the 1.9kb PCR product (not shown). (C) Generation of *hdp1-Ty1* parasites by CAS9 genome editing. Insertion of the C-terminal triple Ty1 epitope tag at the 3' end the *hdp1* coding sequence was confirmed by PCR and checked for mutations by Sanger sequencing of the 1.1kb PCR product (not shown). (D) Generation of *Δhdp1* parasites by CAS9 genome editing. Replacement of 1.4 kb flanking the *hdp1* start codon by a hDHFR selectable marker cassette was confirmed by PCR. (E) Generation of *hdp1-glmS* parasites by CAS9 genome editing. Insertion of the C-terminal triple Ty1 epitope tag and the glmS ribozyme at the 3' end the *hdp1* coding sequence was confirmed by PCR and checked for mutations by Sanger sequencing of the 1.4 kb PCR product (not shown).

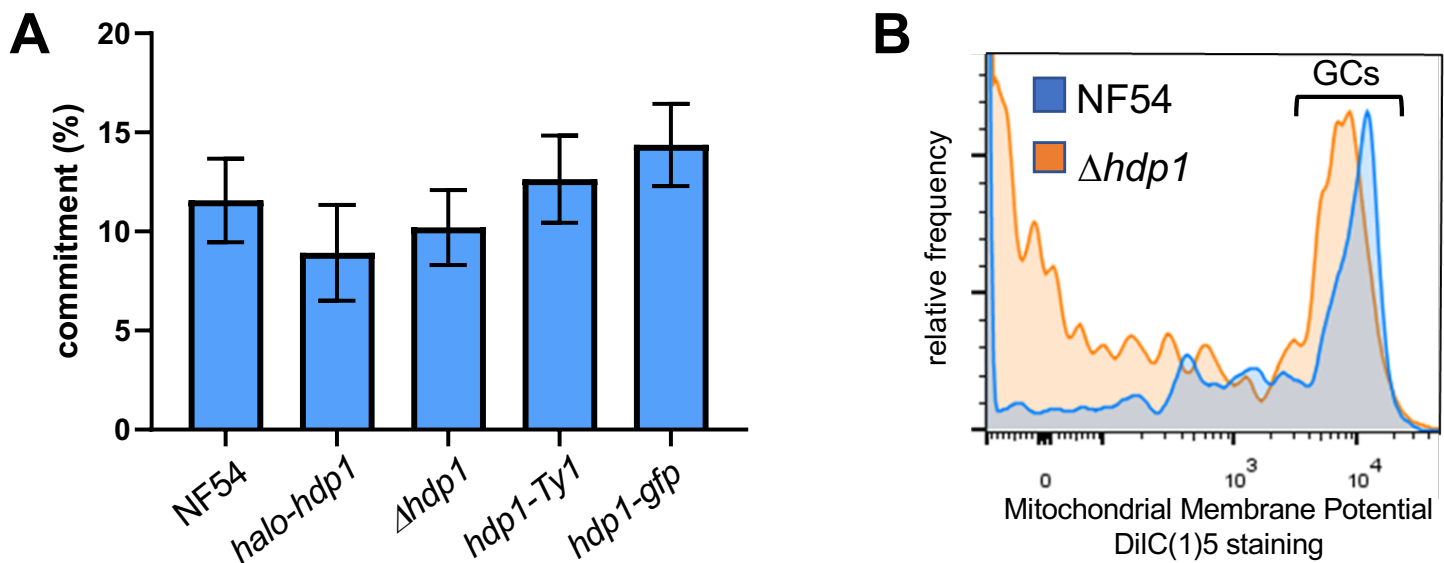


Figure S2: Loss of HDP1 does not alter the sexual commitment frequency or Stage I gametocyte viability. (A) The sexual commitment frequency (day 5 gametocytes per day 1 ring stages) is not significantly affected in *halo-hdp1* and $\Delta hdp1$ parasites. $n=3$ (B) Mitochondrial membrane potential as measured by DiIC(1)5 staining indicates similar viability of day 2 gametocytes (GCs) from NF54 (blue) and $\Delta hdp1$ (orange). Representative of $n=2$.

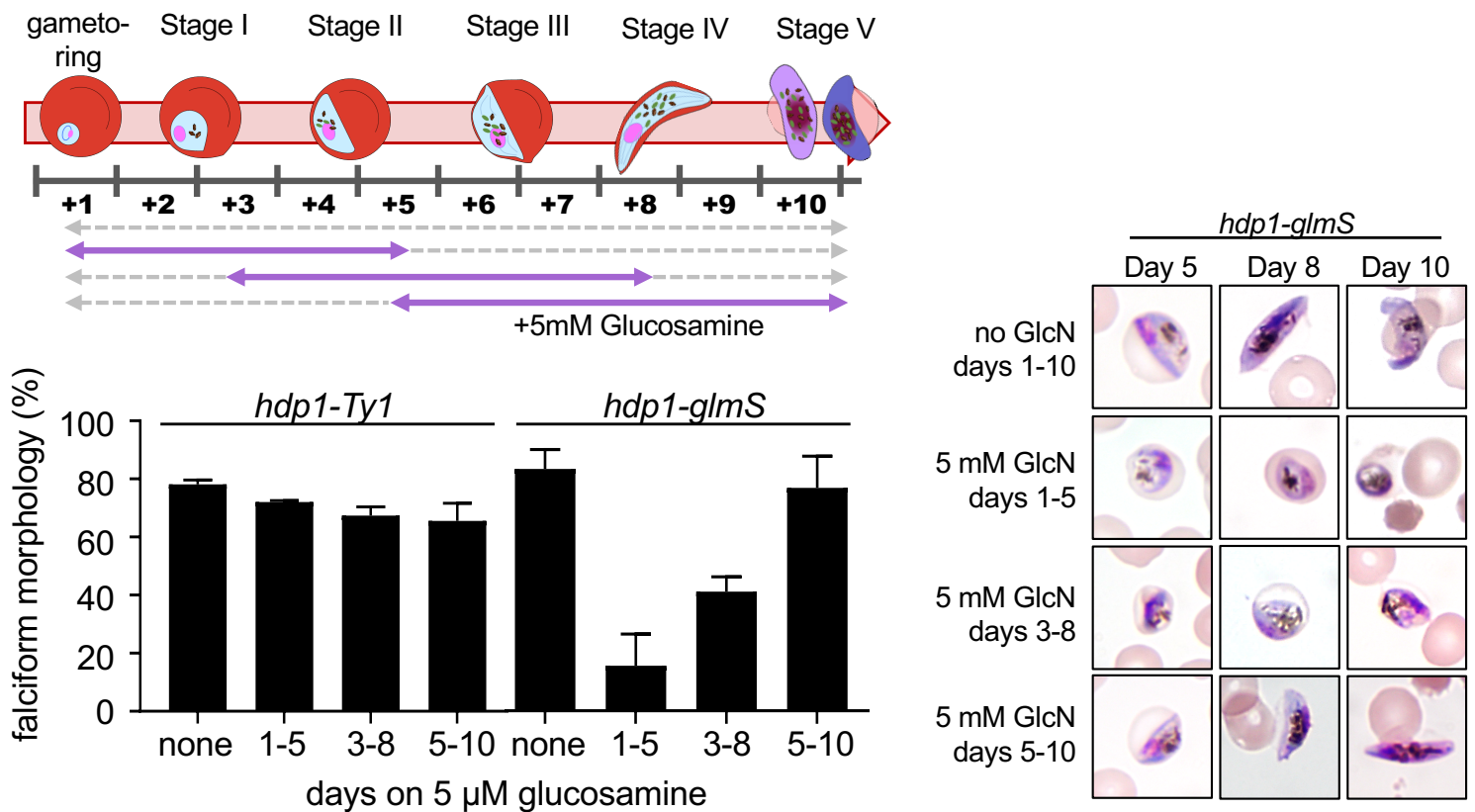


Figure S3: Inducible knockdown of HDP1 reduces gametocyte maturation in early but not late gametocytes. Representative morphology (right) of *hdp1-glmS* gametocytes in response to 5mM glucosamine on days 1-10, 3-8, 5-10, or in the absence of glucosamine. Percentage of falciform gametocytes on Day 10 in response to 5 mM glucosamine on days 1-10, 3-8, 5-10, or in the absence of glucosamine for *hdp1-Ty1* or *hdp1-glmS* parasites (bottom). mean \pm s.e.m of $n=3$.

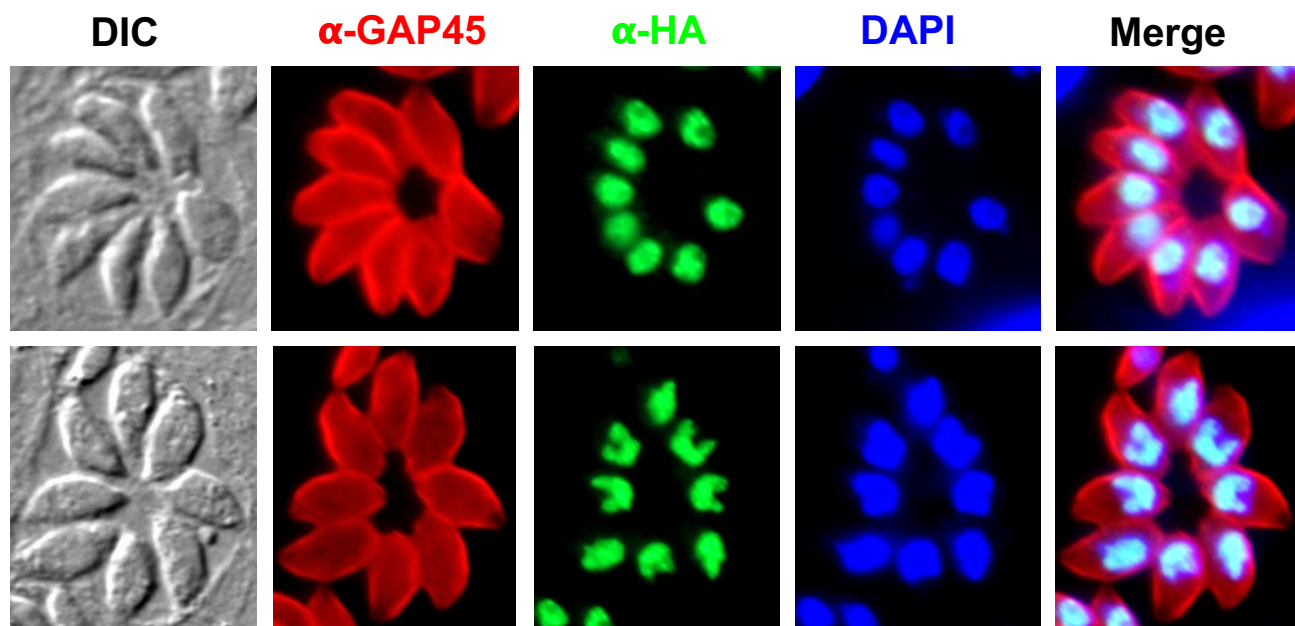


Figure S4: Immunofluorescence microscopy localizes the HA-tagged ortholog TGME49_233160 to the nucleus of *Toxoplasma gondii* tachyzoites.

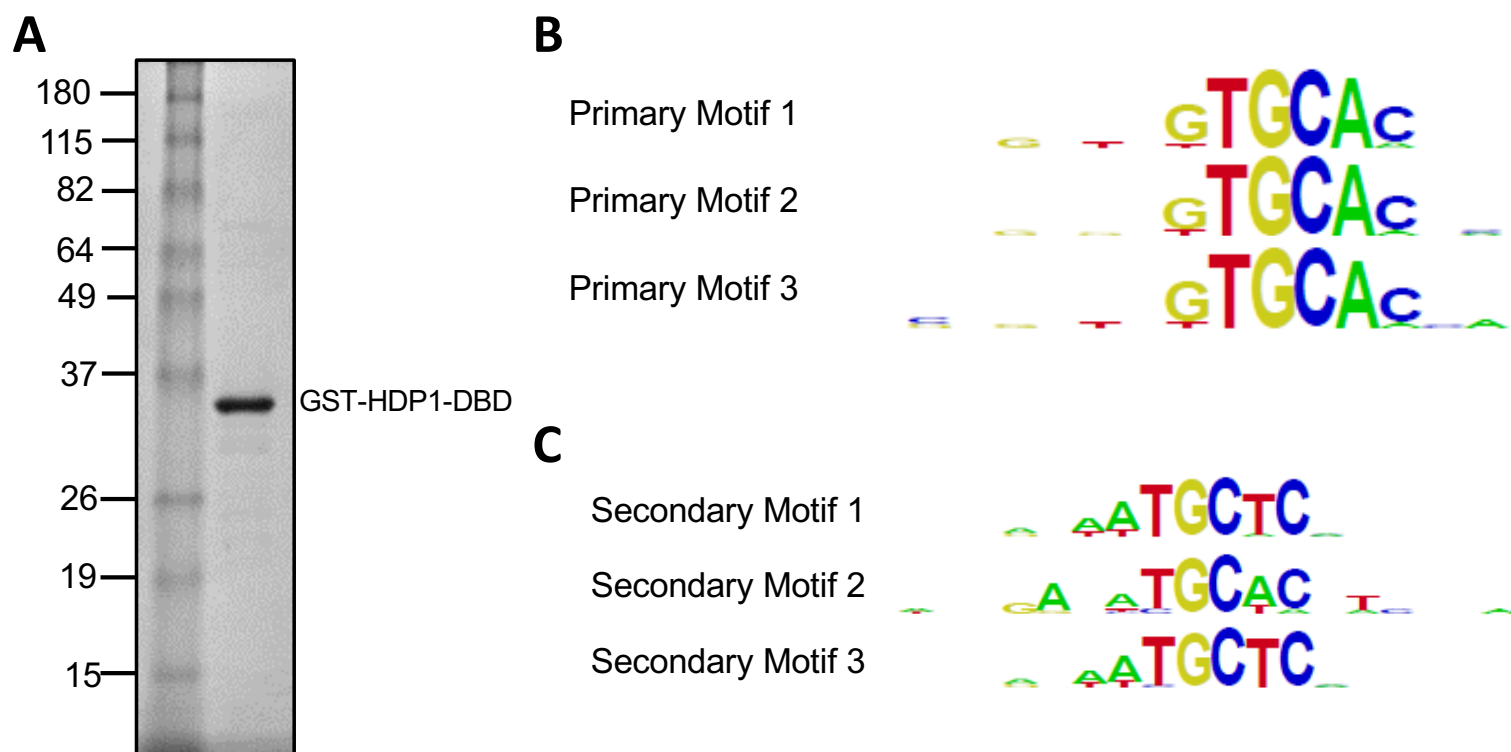


Figure S5: HDP1 binds to a GC-rich motif on Protein Binding Microarray (A) Coomassie stain of GST-HDP1-DBD used for PBM analysis. (B) Top three primary motif hits. (C) Top three secondary motif hits after removal of primary hits.

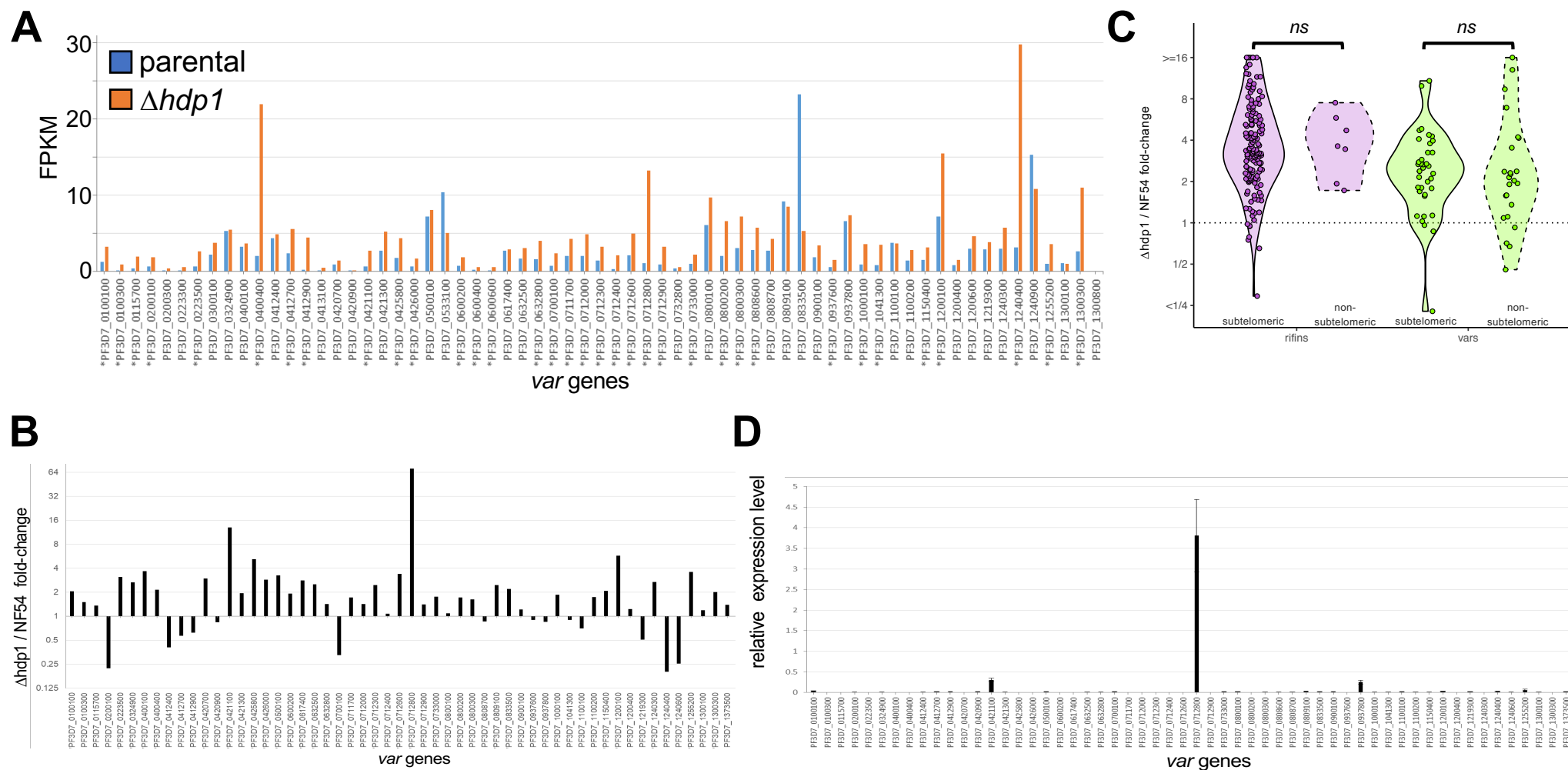


Figure S6: var gene expression is altered in early $\Delta hdp1$ gametocytes but not asexual blood stages. (A) Normalized abundance of reads uniquely mapping to var genes in day 2 gametocytes from $\Delta hdp1$ (orange) or parental NF54 parasites (blue). Significantly upregulated genes are marked with asterisks. (n=2) (B) qRT-PCR confirmation of var gene up-regulation in $\Delta hdp1$ vs NF54 day 2 gametocytes. (C) Upregulation of *rifin* (purple) and *var* genes (green) in $\Delta hdp1$ day 2 gametocytes is independent of chromosomal position in subtelomeric or non-subtelomeric heterochromatin clusters. (D) qRT-PCR analysis of var transcript abundance (normalized seryl tRNA synthetase expression) in $\Delta hdp1$ asexual ring stages found expression a single dominant var as expected indicating that mutually exclusive expression remains unchanged in asexual stages. (n=2)

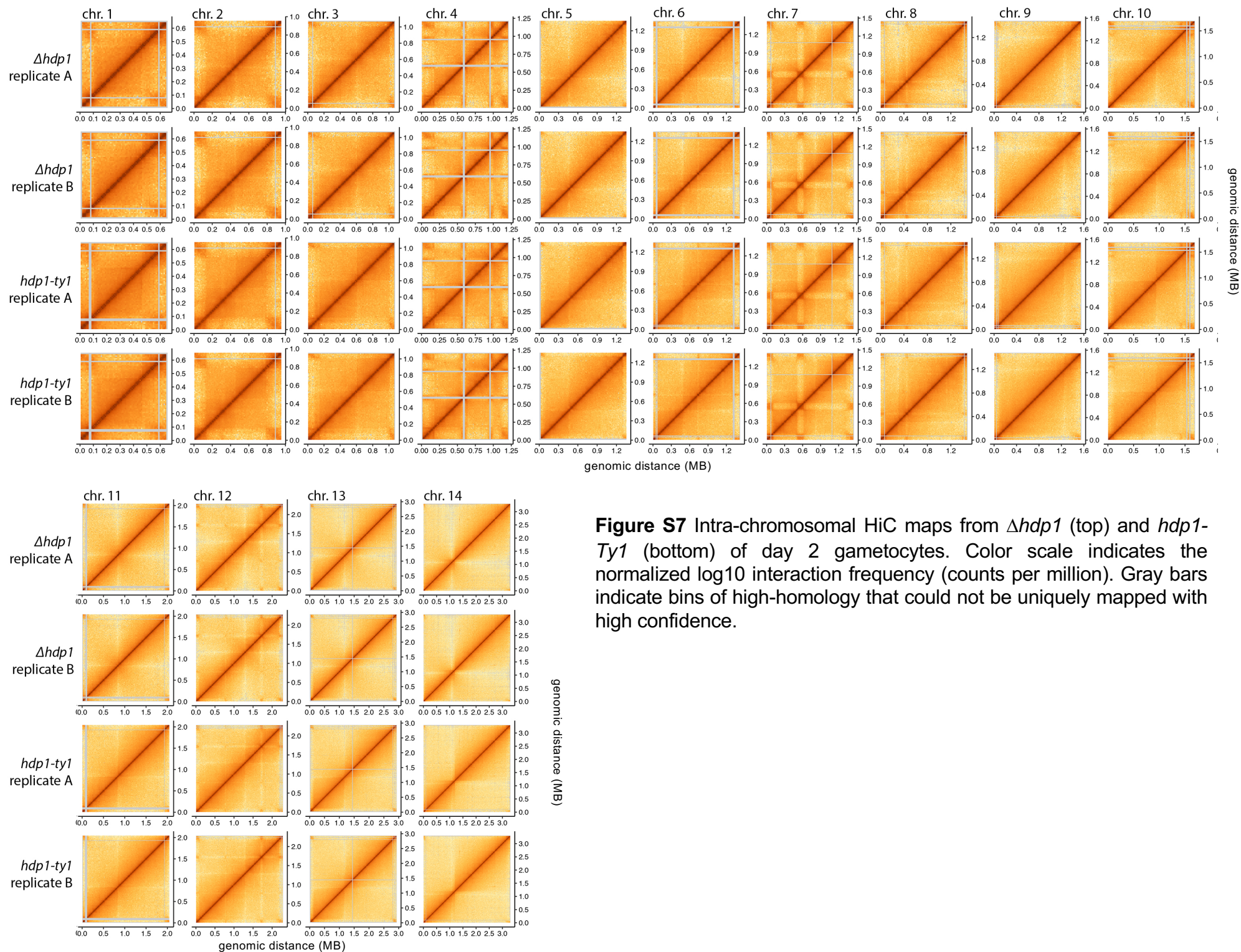


Figure S7 Intra-chromosomal HiC maps from $\Delta hdp1$ (top) and $hdp1$ -Ty1 (bottom) of day 2 gametocytes. Color scale indicates the normalized log10 interaction frequency (counts per million). Gray bars indicate bins of high-homology that could not be uniquely mapped with high confidence.